MASTER'S DEGREE IN MICRO AND NANOTECHNOLOGIES FOR INTEGRATED SYSTEMS

Master's Degree Thesis

Platform for Organ-on-Chip mechanobiological analysis and Stretchable biodegradable electrodes as strain sensor

Supervisors

Prof. Matteo COCUZZA

Tutors

Prof. Clementine BOUTRY

Prof. Daan BRINKS

Candidate

Matteo PIRRO

September 2022

Summary

In last decades the huge development in the synthesis of reliable and effective biodegradable and biocompatible materials and the improvement of microfabrication techniques, have brought a wide increase in neural technologies. These devices can interface and interact with the neural system, especially for medical applications, increasing the healing process for different injuries and diseases. Among such applications, one of the most intriguing is based on scaffolds that help the regrowth and regeneration of peripheral nerves.
In this project, the milestones for the complete design and fabrication of a biodegradable scaffold for the regeneration of peripheral nerves are deposited. Three main characteristics are mandatory for this scaffold: the use of biodegradable material, the presence of integrated stretchable electrodes, and the mechanical stimuli of the nerves to enhance their healing. However, due to the embryonal stage of the project, starting from scratches, the basic steps are needed to be fixed and set. The project is divided into two sub-parts, that were run in parallel.

First, to be able to correctly stimulate nerves and enhance their regrowth, biological studies on neural cells were conducted. Nevertheless, to perform this research, a stage for mechanobiological studies was needed to be designed and fabricated. This part was concerning the development of a platform that allows the controlled application of a radial strain to cell culture. All the different steps were performed, from the physics behind the device to its design, assembly, characterization, and biological validation. The system should be easily reproducible for use in many different laboratories and be highly compatible with a wide variety of imaging systems and biological specimens.

The second sub-part of the project was concerning the development of biodegradable and stretchable electrodes for the recording of the signal and studying the strain in the system. The first target of this section was relying on the synthesis of different biodegradable and stretchable polymers, like POMaC, PGS, and PGSA. Then an electrode pattern has been designed in order to have a stretchable electrode, working also as capacitive strain sensor, finding the most suitable microfabrication technique to deposit them on top of the biodegradable elastomer. Thus, a iron layer deposited by spark ablation was chosen. Finally, to test these devices a setup able to stretch the sample and measure the impedance was built.

Table of Contents

List of Figures

Acronyms

OoC
Organ-on-Chip

POMaC
poly(octamethylene maleate (anhydride) citrate)

PGS
Poly(Glycerol Sebacate)

PGSA
Poly(Glycerol-co-Sebacate)Acrylate

PDMS
Polydimethylsiloxane

IPA
Isopropyl alcohol

GEVI
Genetically Encoded Voltage Indicator

DIC
Digital Image Correlation

ROI
Region of Interest

DMA
Dynamic Mechanical Analysis

HEK293T
Human Embryonic Kidney 293 Tumoral cells

PVA
Polyvinyl alcohol

Chapter 1

Introduction

In the last decades the wide development in material science, with the synthesis of reliable and effective biodegradable and biocompatible materials, and the improvement of microfabrication techniques on them, has brought the development and a large increase in the state of biomedical applications, that can interface with the neural system. Such kinds of applications have been developed especially for medical targets, to help recovery from injuries and from different types of diseases.
Then, between a large number of peripheral neural interfaces (devices that directly interact with the peripheral neural system), one of the most intriguing are scaffolds [1] that can help the regrown and regeneration of peripheral nerves.
This project is the initial part of a much bigger project, the complete design and full development of a biodegradable scaffold, able to help the regeneration of peripheral nerves.
The main characteristics that define this scaffold is, the use of biodegradable material, to make it absorbable by the human body, the integration of electrodes to interface with the neural system, and, finally, it has to mechanically stimulate the nerve [2], to facilitate their repairs and regeneration[3].

However, due to the embryonal stage of the project that starts from scratch, the real basics need to be fixed and set. For these reasons, the project is divided into two sub-parts, that run in parallel.

Firstly, to be able to correctly stimulate nerves to enhance their regrown, biological studies on neural cells need to be conducted. Nevertheless, to do that, a platform for mechanobiological studies needs to be designed and fabricated. The first part, then, is about the development of a stage that allows the application of a radial strain to cell culture in a controlled manner. All the different steps need to be performed, including the concept of the device, design, assembly, characterization, and final biological validation. Ideally, such a system should be easily reproducible for use in many different laboratories and be highly compatible with a wide variety of imaging systems and biological specimens.

The second sub-part of the project, on the other hand, was about the development of biodegradable stretchable electrodes. In particular, the target of this section was

to work on the synthesis process of different biodegradable polymers (POMaC. PGS and PGSA), design a pattern to have stretchable electrodes that can work also as a capacitive strain sensor, and chose the most suitable microfabrication technique. Finally, this kind of device needs to be tested. To do that, a setup able to stretch the sample and measure the impedance was built.
In this case, the objective of the project was to really build the milestone for the development of electrodes as neural interfaces. Better define and test different biodegradable polymers, try to use microfabrication techniques on them (a spark ablation iron layer was finally chosen), design a structure to detect the capacitance variation, and finally develop a setup able to characterize the main behavior of these devices (capacitance vs strain) were the main targets.

1.1 Platform for Organ-on-Chip mechanobiological analysis

Due to the necessity to perform a mechanobiological study on neural cells, but also, in general, on the increasing demand for such kind of device, for OoC studied, a stage that allows to actuate and stretch cells is designed and fabricated.
Several solutions already exist, with different characteristics, materials, and working principles. The idea behind this part of the project was to develop a device simple-to-replicate, but also easy to engineer. All the steps for the development were followed, from the definition of the working principle, the design, the optimization of the assembly process, the characterization through a Digital Image Correlation technique, and finally the validation through biological study (by HEK293T cell culture). The final target is to develop a device reliable and compatible with different imaging systems and biological samples.

1.2 Biodegradable stretchable electrodes as strain sensors

The second part of the project was about the development of a biodegradable stretchable electrode that should work as a strain sensor. The target of this part is to set the milestone for the creation of such kind of devices. The need for a strain sensing mechanism is due to the fact that, in the final scaffold, mechanical stimulation will be present, and feedback on the applied strain is needed.
The first step was, then, to follow the synthesis of different biodegradable materials, which will compose the final scaffold. Three different materials were synthesized.
These materials were then used as a stretchable substrate for the electrodes.
Then a phase of design, to better define the conductive pattern on top of the substrate was needed. The pattern should also work as a strain sensor, in particular, with a capacitance sensitive to the applied elongation.
Finally, a setup able to stretch the sample and measure the capacitance (impedance in general) is built.

Chapter 2

Platform for OoC mechanobiology analysis

2.1 Introduction

Due to the necessity of a platform that allows conducting studies about the mechanobiological properties of cells, a device, simple-to-reproduce and compatible with different types of biological samples is designed.
To be able to develop an efficient scaffold for peripheral nerve repair, a study on the mechanobiological properties of neural cells is essential, to better understand their responses, and how to actuate and increase their regrown. For this reason, such kind of stage was fabricated and validated, with the aim to be adaptable and compatible with different types of imaging systems and biological samples.
The idea is to have a device that can stretch, in a controllable manner, the cell culture on top of it, to analyze their response (depending on the biological culture and on the type of study, such as morphological or electrophysiological). The main target, thus, is to develop such a kind of platform that should be easy to reproduce and engineer.

The basic idea is to have a membrane, on which cells can grow, that deflects under the application of pressure. A chamber with a central pillar is placed on the bottom of such a layer. The negative pressure will cause the deflection of the membrane, causing a strain on top of the pillar, where the surface will be flat.
All the steps needed to be performed. The first phase of concepts and design was done. Then the device was assembled and characterized through a Digital Image Correlation technique. Finally, the platform was validated from a biological point of view with HEK293T (Human embryonic kidney tumoral cell) culture, a standard type of cells for biological studies.

2.1.1 Mechanobiology

In the last decades, many studies focused on cell mechanics, due to the recent advances in nanotechnology, microfabrication, and BioMEMS. This field is extremely relevant because allows the combination of the progress in microtechnologies and imaging

systems to conduct biological studies and to better understand the mechanobiological properties of cells. At the microscopic level, cells are subject to several types of force and deformation, as shown in Fig 2.2. All these different stimuli can affect in a different way the cell responses and behavior. Many types of research have shown how these interactions modulate and change several aspects of cells' functions, also from a biological point of view. Mechanosensitive receptors, that receive and translate mechanical signals into biochemical signals, control how responsive cells are to mechanical inputs [4].

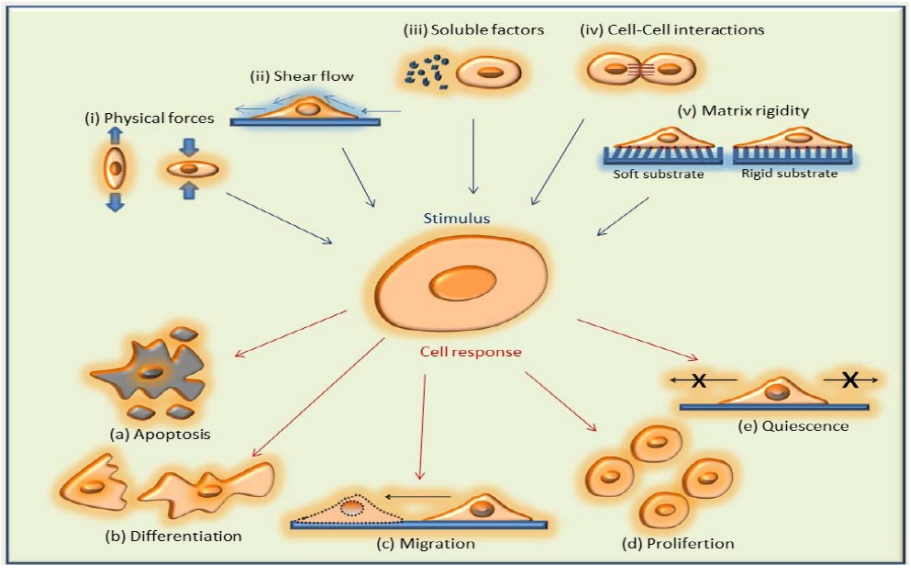

Figure 2.1: Different type of cells stimuli in biological processes and cells responses [5]

Moreover, the combination of new and more precise imaging techniques and BioMEMs provides a huge opportunity to get detailed and accurate results about the mechanobiological properties of cells. Thus, due to the relevance of such a topic, a platform that allows actuating a precise strain on cells and studying their properties was developed and validated. The platform should be not only easy-to-reproduce and reliable but also versatile for different imaging systems and biological samples.

2.1.2 Stretching cells platform

Due to the relevance of such kind of research, many platforms are developed in the past, to actuate and stimulate cells, in various ways. Several techniques were developed in decades, to stimulate and apply also different types of force on cell culture, especially with the advances in microfabrication and BioMEMs [5].
Many reviews were conducted on this wide topic, especially due to the variety of possible solutions and approaches to interact with cells [6], [7].

One of the most common and simple solutions is to apply a pressure (positive or negative) that deflect an elastomer layer, on which organoids are placed. Fig 2.2 shows two existing examples of such kinds of devices. On the right the actuating pressure is negative, while on the left is positive, causing a swelling of the polymer.

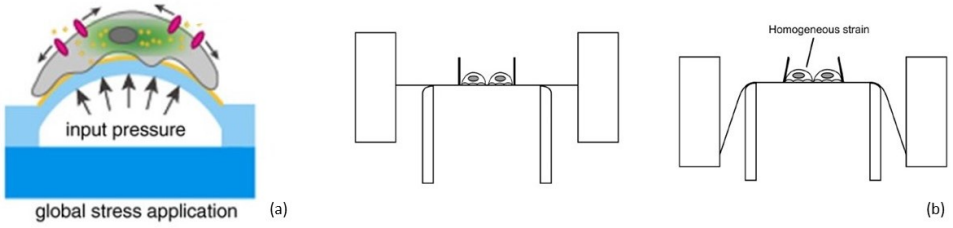

Figure 2.2: Examples do stretching cells device by use of elastomers; (a) Deflection by positive pressure [8]; (b) Deflection by vacuum [9];

Especially, FlexCell [10] is one of the main on-the-market solutions, widely used in mechanobiological applications, that follows the same working principle of a polymeric deflecting membrane, but it is quite expensive.
For all these reasons, a new platform, easy to fabricate, reproducible, versatile and that can be engineered was designed and validated.

2.2 Design and methodology

The basic principle behind the designed device is quite simple. The main aim is to develop a simple, cheap, and easy-to-reproduce platform that allows conducting studies about the mechanobiological properties of different types of cells. Mainly, the device is based on a membrane of soft silicone-rubber, biocompatible material with hyperelastic properties, on which cells could grow. Then, under this plate, a chamber is placed. The aim of the camber is to actuate a vacuum that causes the deflection of the membrane. Moreover, in the center of the chamber, a circular pillar is placed. The silicone layer is attached to the chamber only on the edge, while there is no direct bound with the pillar. The idea, thus, is to apply negative pressure through two inlets, to have a more uniform distribution of the applied force. The membrane deflection will provoke a planar radial stretch on top of the pillar itself.

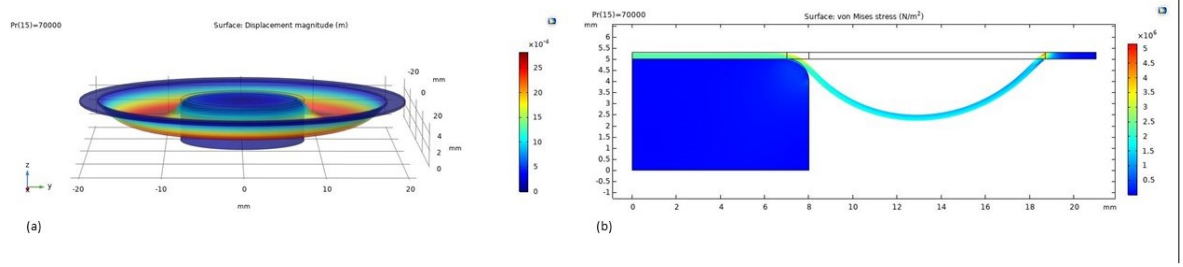

Figure 2.3: Comsol simulation results of membrane deflection for cells culture (applied negative pressure of 70 kPa); (a) 3D view of stress distribution (b) Lateral 2D view of stress distribution, with axial rotational symmetry

Fig 2.3 shows the circular pillar with the deflected membrane on top. The surface on top of the pillar itself will be subject to a uniform radial strain.

To be able to have such kind of device a first step of design is needed. Through Comsol simulations, optimization on the geometrical dimension of the dish is reached but especially this step was required to check and extract:

- the relation between the applied pressure and the radial strain on the soft silicone plate;
- the uniformity of the radial strain all over the top surface;
- general response (vertical displacement, stress distribution);

One of the most relevant points was to have a uniform and constant radial strain all over a certain region, to make all the cells sense the same stretch. Other interesting aspects of the stage's behavior were analyzed, such as the stress distribution and the vertical displacement, to better understand the total behavior and response of the device.
Moreover, due to the hyperelastic properties of the material, a first attempt was done using values from the literature. However, to have a more precise knowledge of the material properties, a DMA test was performed and different hyperelastic models were extracted and computed (Neo-Hookean, Ogden, and Mooney-Rivlin). Then other simulations were performed based on the real extracted data. Finally, the Ogden model was used as a reference, providing the best fitting in the hyperelastic characteristic of the material.

2.2.1 Strain theory

Thus, the cell will grow on the soft silicone-rubber layer, and, with the deflection of this membrane, different strains will be created on the dish. Firstly, a decision on the strain to be applied should be made. For the type of cells under study (HEK293T for the current study and Neural Progenitor Cell for the future), an equibiaxial strain should be applied. This choice is made based on the fact that NPCs grow in a radial way from the center of the pillar, so to actuate and stimulate them, the best solution is to have a constant radial displacement from it, while the study with HEK293T is conducted especially to validate, from a biological point of view, the device. For this reason, a circular shape of the pillar is chosen, to have, theoretically, a uniform radial strain, being the pressure uniform all around it. Also, by changing the shape of the pillar, making it ellipsoidal, should be possible to have a uniaxial strain, extremely useful for other types of specimens and studies. The strain, in a very straightforward way, can be defined as:

$$\varepsilon = \frac{L^{'} - L_0}{L_0} = \frac{\Delta L}{L_0} \tag{2.1}$$

However, giving a deeper understanding of this concept, the strain is defined as a tensor (Cauchy strain tensor), in which each component is equal to:

$$\varepsilon_{i,j} = \frac{1}{2}\left(u_{i,j} + u_{j,i}\right) \tag{2.2}$$

where i, j represent the different coordinates.
So, expressing it as a tensor and in the cartesian coordinate [11], it is possible to write:

$$\begin{bmatrix} \varepsilon_{xx} & \varepsilon_{xy} & \varepsilon_{xz} \\ \varepsilon_{yx} & \varepsilon_{yy} & \varepsilon_{yz} \\ \varepsilon_{zx} & \varepsilon_{zy} & \varepsilon_{zz} \end{bmatrix} = \begin{bmatrix} \frac{\partial u_x}{\partial x} & \frac{1}{2}\left(\frac{\partial u_x}{\partial y} + \frac{\partial u_y}{\partial x}\right) & \frac{1}{2}\left(\frac{\partial u_x}{\partial z} + \frac{\partial u_z}{\partial x}\right) \\ \frac{1}{2}\left(\frac{\partial u_y}{\partial x} + \frac{\partial u_x}{\partial y}\right) & \frac{\partial u_y}{\partial y} & \frac{1}{2}\left(\frac{\partial u_y}{\partial z} + \frac{\partial u_z}{\partial y}\right) \\ \frac{1}{2}\left(\frac{\partial u_z}{\partial x} + \frac{\partial u_x}{\partial z}\right) & \frac{1}{2}\left(\frac{\partial u_z}{\partial y} + \frac{\partial u_y}{\partial z}\right) & \frac{\partial u_z}{\partial z} \end{bmatrix} \tag{2.3}$$

However, in the application under investigation, the cells grow in a radial way, so the target is to have somehow a radial strain uniform and constant in a well-known region. Expressing the strain tensor in cylindrical coordinates:

$$\begin{bmatrix} \varepsilon_{rr} & \varepsilon_{r\vartheta} & \varepsilon_{rz} \\ \varepsilon_{\vartheta r} & \varepsilon_{\vartheta\vartheta} & \varepsilon_{\vartheta z} \\ \varepsilon_{zr} & \varepsilon_{z\vartheta} & \varepsilon_{zz} \end{bmatrix} = \begin{bmatrix} \frac{\partial u_r}{\partial r} & \frac{1}{2}\left(\frac{1}{r}\frac{\partial u_r}{\partial \vartheta} + \frac{\partial u_\vartheta}{\partial r} - \frac{u_\vartheta}{r}\right) & \frac{1}{2}\left(\frac{\partial u_r}{\partial z} + \frac{\partial u_z}{\partial r}\right) \\ \frac{1}{2}\left(\frac{1}{r}\frac{\partial u_r}{\partial \vartheta} + \frac{\partial u_\vartheta}{\partial r} - \frac{u_\vartheta}{r}\right) & \frac{u_r}{r} + \frac{1}{r}\frac{\partial u_\vartheta}{\partial \vartheta} & \frac{1}{2}\left(\frac{\partial u_\vartheta}{\partial z} + \frac{\partial u_z}{r\partial \vartheta}\right) \\ \frac{1}{2}\left(\frac{\partial u_z}{\partial r} + \frac{\partial u_r}{\partial z}\right) & \frac{1}{2}\left(\frac{\partial u_z}{r\partial \vartheta} + \frac{\partial u_\vartheta}{\partial z}\right) & \frac{\partial u_z}{\partial z} \end{bmatrix} \tag{2.4}$$

In case of axial rotational symmetry, considerable simplification should be taken into account, especially it is possible to assume: $u_\vartheta = 0$ and $\frac{\partial}{\partial\theta}[\,] = 0$.
These equations make the matrix and the components of the tensor much simpler.

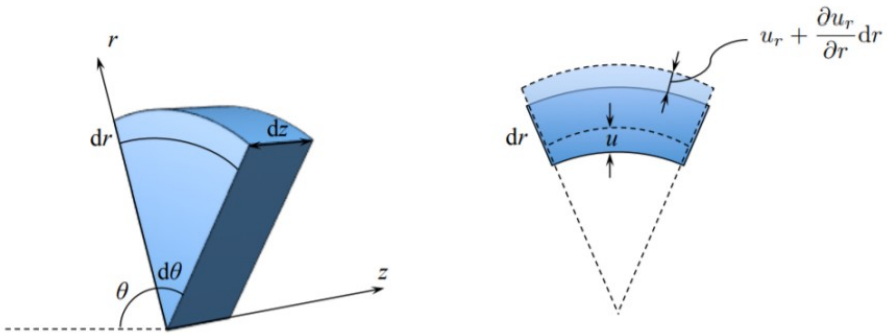

Figure 2.4: Cylindrical coordinates and change in length in the radial direction [12]

From this formulation, the crucial value is given by $\varepsilon_{r,r}$, which is the one to extract from Comsol simulation and, one of the main targets of this simulation phase is to find the relationship between this value (radial strain) and the applied pressure, to exactly know which value should be kept on the bottom of the membrane to have the wanted strain on top of it.

Moreover, it is important to take into account how the displacement is bonded to the strain [13], in particular the strain can be defined as the derivative of the displacement. From simulation, it is possible to extract in a direct way the displacement field, but not the radial strain. Thus, the radial displacement field is related to the strain by:

$$\varepsilon_{r,r} = \frac{R_2' R_1' - R_2 R_1}{R_2 R_1} = \frac{u_r\left(r + \Delta r, \vartheta, z,\right) - u_r\left(r, \vartheta, z,\right)}{\Delta r} = \frac{\partial u_r}{\partial r} \tag{2.5}$$

Where, considering two points in space, which coordinates are expressed in cylindrical one R_1 and R_2, they are separated by a radial distance that is equal to the distance of the two radial components of the coordinates. When a strain is applied the radial distance change by the relations $r^{'} = r + u_r\left(r, \vartheta, z\right)$ where u_r is the radial strain, a function that, depending on the coordinates express, how much a point changes its radial components. Thus, it is possible to consider that the radial strain is equal to the derivative of the radial displacement (with respect to the radial position, r). For this reason, one of the targets of these simulations is to check that on a specific region (on top of the pillar) the radial strain is uniform, and this is given by a linear radial displacement. A linear radial displacement provides a radial strain that is constant, and so uniform, all over the region under study.

Moreover, taking into account a simple radial strain $\varepsilon_{r,r}$, without any circumferential strain, and considering a radial section, as in Fig. 2.4, the initial area of the section, equal to A_r, will increase of a value $\left(1 + \varepsilon_{r,r}\right)^2$; thus $A_r' = \left(1 + \varepsilon_{r,r}\right)^2 A_r$. This increase will be relevant in the cell study, as a reference to the area increment.

2.2.2 Hyperelastic model

The main significant characteristic that led to defining a material as hyperelastic is the significant nonlinear elastic deformation. Because there is no internal energy loss in either linear or hyperelasticity, the work done during the loading process is entirely recovered when the load is released. The distinction is that for hyperelastic materials, the strain-stress relationship is nonlinear and the deformation can be quite significant.
Thus the most significant aspects of hyperelastic materials are:

- subjected to large strain and constitutive law model non-linear
- typically elastomers and biological tissue
- the stress-strain relationship is derived from a strain energy density function (W_s) stress does not depend strongly on strain rate or strain history

For hyperelastic materials, the stress-strain relationship is derived using a function called the Helmholtz free energy per unit reference volume [14]. It is a scalar-valued function that connects the strain energy to the state of deformation and goes by the names of strain energy density, strain energy function, or elastic potential. Hyperelastic materials have the special property that their strain energy density depends only on the current strain and not on the previous loading. The creation of a proper strain energy density function is the first step in the construction of hyperelastic material

models. The strain energy function is determined under a number of assumptions, such as homogeneous substrate, nearly or completely incompressible material, and no hysteresis behavior. Various research teams have developed many constitutive models for hyperelastic materials throughout the years. The models can be characterized as either phenomenological or micromechanical [15] depending on how they are developed. Phenomenological-based models, as their name implies, are developed by observing rubber-like materials subjected to various homogeneous deformation situations and then applying mathematical equations to the obtained experimental data. On the other hand, to characterize the behavior of hyperelastic materials at the microscopic and macroscopic levels, micromechanical models make use of statistical mechanics approaches. Despite the fact that phenomenological models account for a greater proportion of hyperelastic models in the literature, micromechanical-based models have drawn more interest since their governing parameters can link the mechanical behavior with the physical or chemical structure of the material.

Thus, hyperelastic materials are characterized by their elastic strain energy W_s, known also as energy density, which allows for describing the non-linear relation between stress and strain, as opposed to Hooke's law in linear elasticity. Moreover, this value is linked to the Piola-Kirchhoff stress by the equation:

$$P = 2\frac{\partial W_s}{\partial C} \tag{2.6}$$

where C is the Cauchy-Green deformation tensor and the strain energy density can be written as a function of this value $W_s(C)$.
Each hyperelastic model provides a different formulation of this strain energy density, that bring also to a different expression of the Piola-Kirchoff stress. Thus, each one of these models is characterized and defined by various parameters that allow the description of the behavior and response of the elastomer.
Mainly three models are taken into consideration for the modelization of the soft silicone characteristic: Neo-Hookean, Mooney-Rivlin, and Ogden.

The Neo-Hookean is the most commonly used and well-known hyperelastic model due to its simplicity as it requires only two material parameters that can be easily determined [16]; the shear modulus and the bulk modulus. With the Neo-Hookean it is possible to express the Piola-Kirchhoff stress (in case of uniaxial deformation) as:

$$P_{uniaxial} = \mu\left(\lambda - \lambda^{-2}\right) \tag{2.7}$$

where λ is defined as the actual length over the rest length (so equal to 1 when no strain is applied and increases with the elongation).
Generally, in the formulation of this model, only the shear modulus value is computed, μ, while the bulk's modulus is assumed from the literature, due to the fact that in this formulation of the stress only μ appears.

The second model taken into account was formulated by Mooney [17] and Rivlin[18] and has a reputation for predicting the response of hyperelastic materials to a high level of accuracy, therefore, it is very well known. In this case, the stress can be expressed as:

$$P_{uniaxial} = 2\left(1 - \lambda^{-3}\right)(\lambda C_{10} + C_{01}) \tag{2.8}$$

In this formulation the parameters to extract are C_{10} and C_{10}.

Finally, Ogden [19] is a versatile hyperelastic model that can describe the mechanical behavior of a wide variety of materials when subjected to high strains. The energy density function can be written in numerous ways. The predicted stress–stretch response of the Ogden model has been found to agree very well with the classical experimental results. The model is highly suitable for predicting large deformation behavior.

$$P_{uniaxial} = \sum_{p=1}^{N} \mu_p \left(\lambda^{\alpha_p - 1} - \lambda^{\frac{\alpha_p}{2} - 1}\right) \tag{2.9}$$

Thus from this introduction of different models, several comparison studies were executed, in particular, from the data of [20].

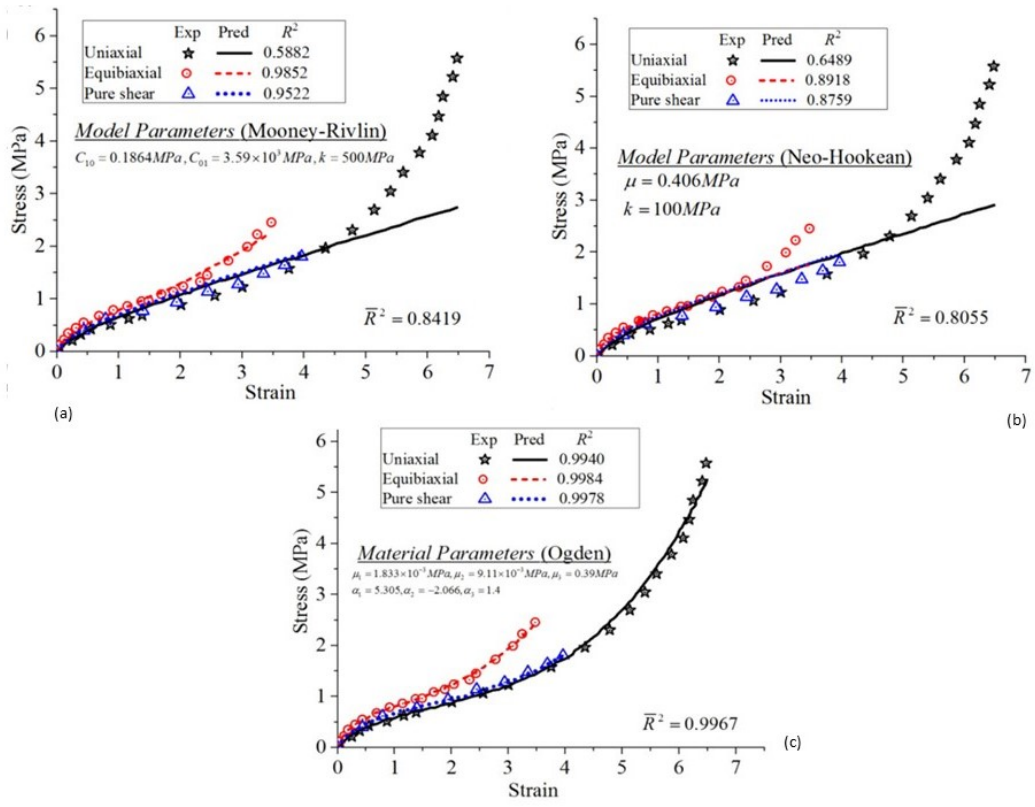

Figure 2.5: Literature comparison of hyperelastic model fitting [15]; (a) Mooney-Rivlin model and parameters; (b) Neo-Hookean model and parameters; (c) Ogden model and parameters

As emerges from Fig. 2.5, the Neo-Hookean model, even if is the simplest one, provides the worst prevision compared to the Ogden and Mooney-Rivlin. On the other

hand, the Ogden one seems to be the model that better describes and characterizes hyperelastic behavior.

2.2.3 Simulation

The system was then constructed on Comsol, to extract its behavior and the main response to negative pressure. The component described in the software was simplified, due to the fact that some parts are not useful from a simulation point of view and also using the symmetry of the structure. Being a circular structure, it can be described as a 2D shape component that rotates around its rotational axis. This axis is the vertical line (**z-direction**) that goes through the center of the structure, so through the center of the chamber and the silicone-rubber layer. Using this type of symmetry, only a 2D component was defined, in the yz plane. Then, the rotational symmetry was used.

To simulate an easy structure only the essential part is taken into consideration. Thus, the main components are the silicone-rubber layer and the pillar on the bottom of it. The edge of the membrane is fixed, so boundary constraints need to be added. Same for the pillar, which bottom and lateral surfaces are not subject to any displacement.

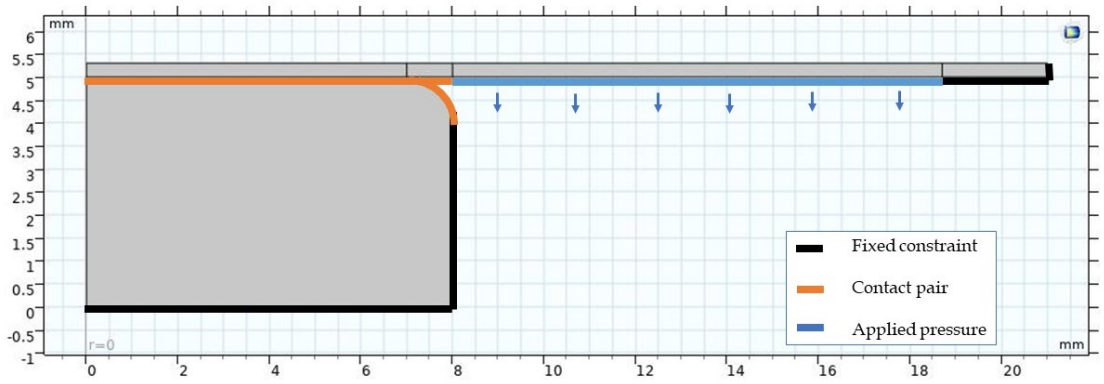

Figure 2.6: Comsol component with the main Solid mechanic constraints

The top rectangle is the silicone membrane, while the bottom one is the pillar, made of though PLA. Some of the main dimensions of the structure are:

- thickness of the silicone-rubber layer = 100 μm and 300 μm
- radius of the silicone-rubber layer = 19 mm
- radius of the pillar = 7.5 mm

About these dimensions, two different thicknesses were chosen to have two different sensitivity and ranges of reachable strain. The radius of the dish itself is the same as other Petri dishes on the market and commonly used. Moreover, in the simulation an extra ring of silicone was added, so a bigger radius is taken into account. This

is because it will be the part attached and bonded to the bottom chamber, so as to have a more accurate definition of the fixed boundary edge. Furthermore, some important constraints have to be considered, as shown in Fig.2.6:

- the edge of the membrane is fixed because they are permanently bonded to the chamber, so a fixed constraint is added;
- the pillar is part of the chamber, so it is fixed and not subjected to any movement. Another fixed constrain is to be taken into account;
- the axial symmetry is used to simplify the structure; the rotation axis is the vertical one, on the left edge of the structure, where r = 0;
- the negative pressure is applied to the bottom part of the silicone-rubber, that is not in contact with the pillar;
- the link between the pillar and the membrane is not a union, but just a simple contact. This is due to the fact that these two parts are not in any way bonded, but just in contact and the silicone layer will slide on top of the pillar, when the vacuum is applied.

Another very important aspect to consider is the fact that the soft silicone is a hyperelastic material. This brings us to introduce another constraint: define this component as hyperelastic. To describe its behavior, in the first moment, a Neo-Hookean model is used. The main parameters to define (first Lame parameter and bulk's modulus) are taken from literature, looking for some reasonable value that describes the silicone-rubber, in particular, a bulk's modulus of 1.5 GPa was used (from material properties) and a Lame parameter μ of 5.1 MPa. However, this was a temporary modelization because it is very hard to find parameters that can describe accurately these materials *a priori*, so a further step was to execute the DMA test on the membrane material and extract the real parameters of the layer, to have a better description of its behavior. This process was also made through Comsol, by the use of the *Optimization module*, that from the stress-strain curve, with a proper definition of the model and of the equations, allows extracting the wanted parameters of the chosen hyperelastic model.

Then the pressure was applied and a parametric study on it was executed. The pressure was negative, to cause a deflection toward the ground of the membrane. For the two thicknesses, two different pressure are reached. For the 300 μm a maximum pressure of 70 kPa (because it's the maximum value reachable by the vacuum pump available in the lab), while for the 100 μm 40 kPa. Finally, the mesh should be defined very carefully due to the presence of a hyperelastic modulus. The destination mesh, in the contact pair, has to be at least twice as fine as the source. Moreover, the mesh should be properly defined also to capture the hyperelastic behavior of the component. The model runs only if with a penalty factor very small.

2.2.4 Simulation results

Then the study of the device was executed. Mainly, the aim of the simulations was to analyze:

- distribution of the radial displacement, check that has a linear increase from the center of the pillar;
- if any vertical displacement is present. It could be a relevant factor for the focus of the microscope study;
- stress distribution on top of the pillar;

Fig. 2.7 shows some of the main results for a membrane thickness of 300 μm. What is really important to notice is that the radial displacement has a linear increment from the center of the pillar to the edge. This linear increment brings a radial strain that is uniform in the studied region. This means that, when the pressure is applied, on top of the circular pillar a radial strain is created, with a constant value all over the flat surface, due to the fact that the radial strain is equal to the derivative of the radial displacement. However it is important to highlight how close to the edge of the pillar the linear behavior stops. This means that in that region the radial strain is no more constant. Thus, a uniform radial strain is guaranteed on a circular region with a radius of approximately 6 mm on top of the pillar.
Another important aspect is the stress distribution on the pillar surface. As it is possible to see from the results, the stress is constant in all this zone, but rapidly increasing approaching the edges of the pillar. Moreover, in the designed structure, the edge of the pillar are rounded, especially to limit this effect and to contain the increase of stress on the silicone-rubber membrane in the proximity of the pillar edges.
Finally, also a comment on the vertical displacement is needed. Especially, for low pressure (in modulus) there is a small lift of the membrane on top of the pillar. Even if this vertical movement does not affect the radial strain, should be taken into account during the imaging at the microscope with cell culture on top, because it probably will bring a small change in the focus.

Better analyzing the radial displacement, and computing for each pressure value, the derivate of the radial displacement function, it was possible to extract the radial strain, as a function of the pressure. In this way, with a Matlab code, in post-processing, for each value of pressure was possible to associate the strain value present on top of the pillar, and define the pressure-radial strain relation.

Fig. 2.8 show this relation. For a specific value of applied pressure, it is so possible to know the resultant radial strain value. Also, it is important to highlight how the response is characterized by good linearity.

However, the modelization of the material could be inaccurate, due to the fact that the hyperelastic model and parameters were found in the literature. To have a better description of the structure a DMA test was executed on a sample of 100 μm and on 300 μm. This test was needed to extract the stress-strain curve, that with the use of the *Optimization module* of Comsol, can provide the real hyperelastic parameter of the materials.

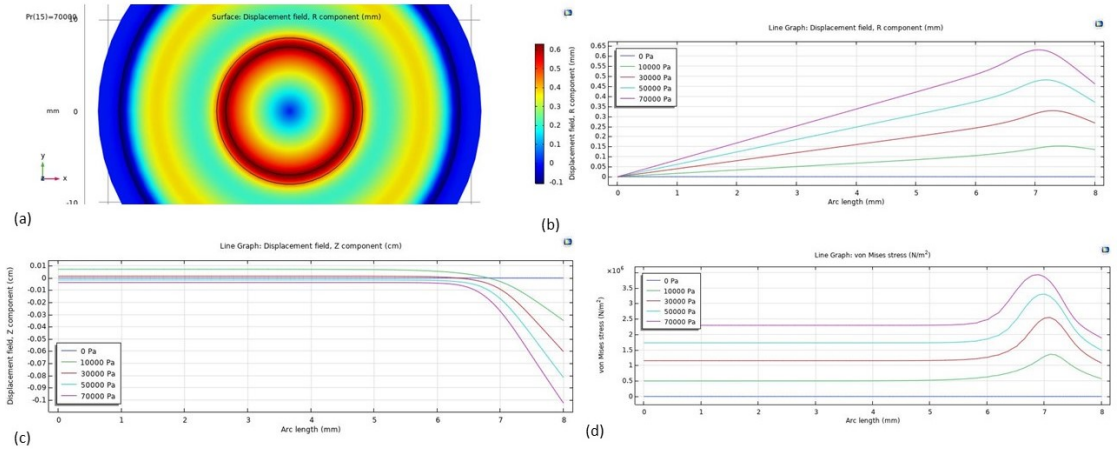

Figure 2.7: Comsol simulation results for membrane thickness 300μm. (a) 2D top view radial displacement; (b) Radial displacement on top of the pillar from the center to the edge; (c) Vertical displacement on top of the pillar; (d) Stress distribution on top of the pillar

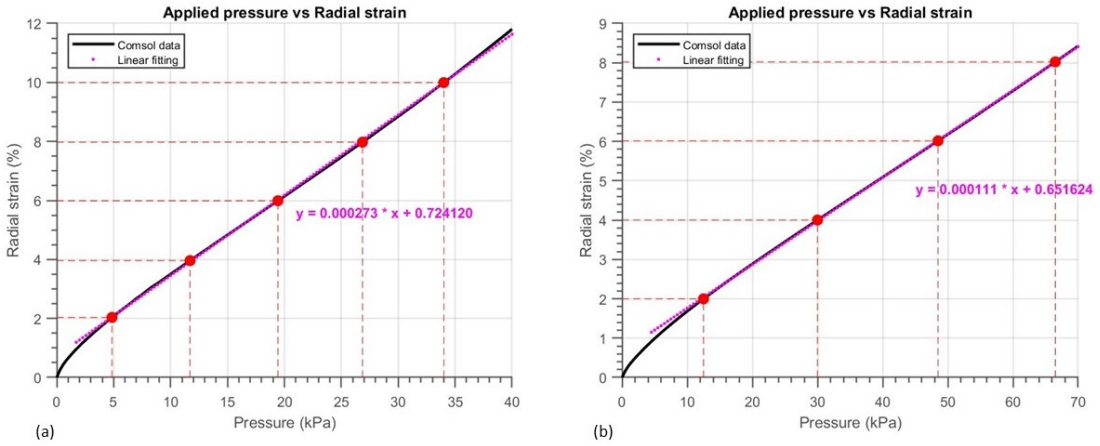

Figure 2.8: Extrapolation of the pressure vs radial strain, with pressure values to apply to have common radial strain values; also the linear fitting equation is described. (a) Thickness of 100 μm thickness; (b) Thickness of 300 μm thickness;

In particular, Fig. 2.9 shows the real stress-strain curve, but also the one computed with the extracted hyperelastic parameters. For both thicknesses, the best approximation is given by the Ogden model as expected. All the main extracted parameters of these models are reported in Fig. 2.10.

Then the simulation was launched again, but now with the real extracted parameters. In particular, for each model, the pressure vs radial strain curve was extracted again, and the comparison was shown in Fig. 2.11.

From this analysis, the Ogden response was chosen as a reference, due to the fact that is the model that provides the best fitting in the hyperelastic behavior. So, after this simulation and design phase, the (theoretical and expected) behavior and the response of the device are well known.

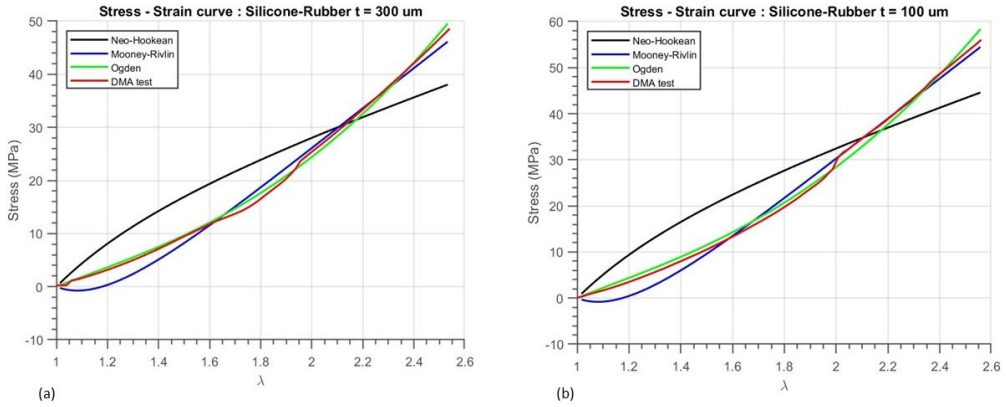

Figure 2.9: Stress-strain curve for silicone-rubber foil, and comparison with different hyperelastic models. (a) 300 μm thickness; (b) 100 μm thickness;

Ogden Model	Thickness = 100 um	Thickness = 300 um
μ_1 (MPa)	3.9700	3.2234
α_1	3.8677	3.9459

Mooney-Rivlin Model	Thickness = 100 um	Thickness = 300 um
C_{10} (MPa)	20.954	18.166
C_{01} (MPa)	-24.605	-21.411

Neo-Hookean Model	Thickness = 100 um	Thickness = 300 um
μ (MPa)	18.552	16.012

Figure 2.10: Parameter from the different models for two thicknesses

2.3 Fabrication

The final fabrication and assembly of the dish should follow an easy and simple-to-replicate process. Mainly three parts are needed: the bottom chamber, the rubber layer, and the wall to put on top of the plate, to close it. The chamber and the wall need to be quite stiff, and for this reason, they are 3D printed, by an Ultimaker Cura 2+, and Though PLA was chosen as the material. On the other hand, the membrane was cut from an on-the-market foam of soft silicone. Finally, they are assembled and bonded together, through the use of PDMS as glue and PSA tape.
In the assembly process, several attempts were made and an "experimental" approach was followed. This process was to arrive at and define a precise series of steps to follow to have a platform reliable and easy to construct, but that has also to behave as expected.

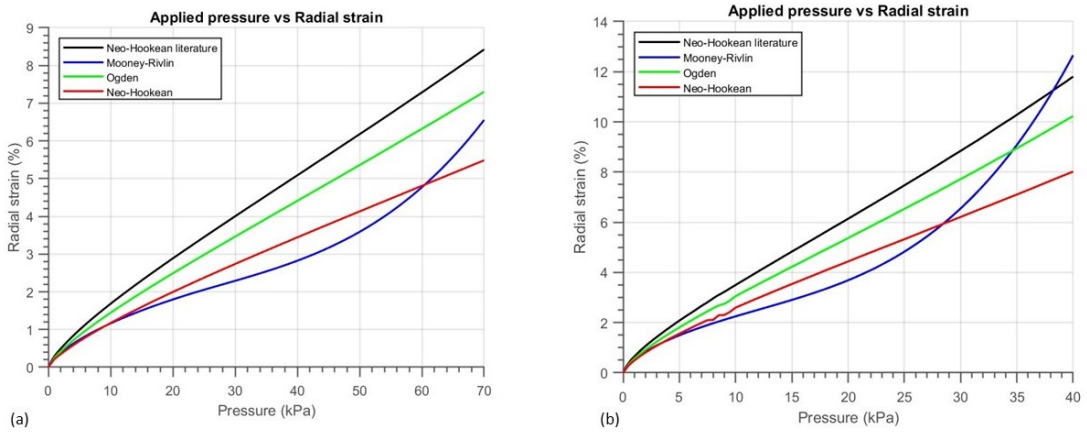

Figure 2.11: Comparison response pressure vs radial strain for the different models; (a) 300 μm thickness (b) 100 μm thickness

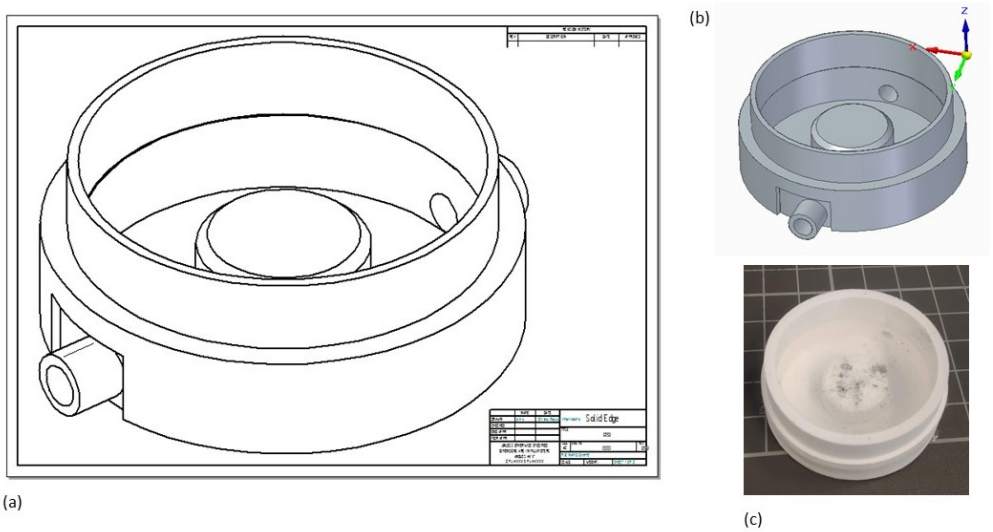

Figure 2.12: Total device; (a) Design paper SolidEdge; (b) 3D view design; (c) Real device after image processing characterization

2.3.1 Material

Two main materials are used for the fabrication: soft silicone and Though PLA. However to bond them and have a stable and reliable device also PDMS and PSA tape are used.

Silicone This material was chosen for the fact that is cheap and easy to find on the market. Moreover, hyperelasticity was one of the main characteristics to look for. One of the key points of this material, obviously, is the fact that has to be biocompatible, to assure cells live and grow on top of it.
However, the adhesion on top of it, for the cells, is very low, due to its hydrophobicity and microscopic roughness. Nevertheless, it does not affect the final validation of the device, due to the use of an adhesion layer, made of fibronectin, that increases

the quality of the cells' adhesion, without effect too much the mechanical properties.

From the original foil, a specified shape is cut, by a precision blade cutter (Silhouette Cameo 4) and then placed on top of the chamber.

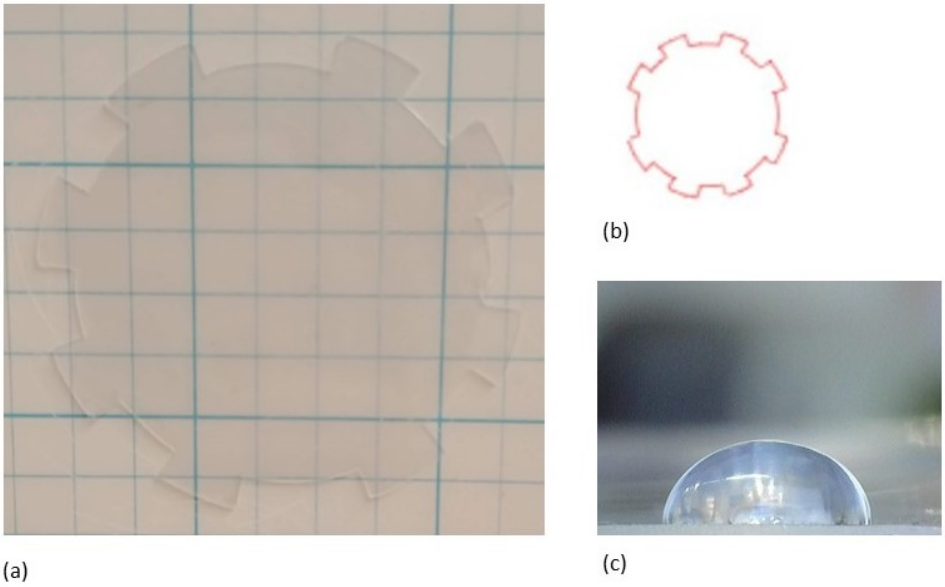

Figure 2.13: Silicone-rubber membrane; (a) Cut membrane; (b) 2D design; (c) Contact angle image

As shown in Fig. 2.13, the shape is a circular one but with some wings. This choice is made to have better adhesion and stability when bonded to the bottom chamber, limiting the movement and eventual sliding on the edge by the rubber layer.
Moreover, the contact angle was measured, by image acquisition with a Dino microscope and ImageJ software as tools for the computation. An angle of 98.3° was measured, demonstrating the hydrophobicity of the material (contact angle $> 90°$).

Though PLA The other two main parts are printed with a 2+ Ultimaker Cura 3D printer. The main characteristic of this material is that is biocompatible but also degradable. The degradability is an aspect to take into account for long-term study but also for the process of sterilization. The best process should be chosen to avoid and limit the acceleration of this process. In general, the time of degradation is quite long and should not affect the use in cell culture and bio applications. For these reasons, the sterilization process was well defined and described, as protocols, to start the cell culture.

These two main parts (Fig. 2.14 and Fig. 2.15) basically are inserted one into another (with the silicone-rubber layer in between), so the wall will cover all parts of the chamber, to guarantee good isolation and avoid any leakage.

Another extremely important aspect of this kind of application is the choice of color. Different colors are available for this material, so a choice about it should be done to optimize the imaging with the microscope. Obviously, the best solution

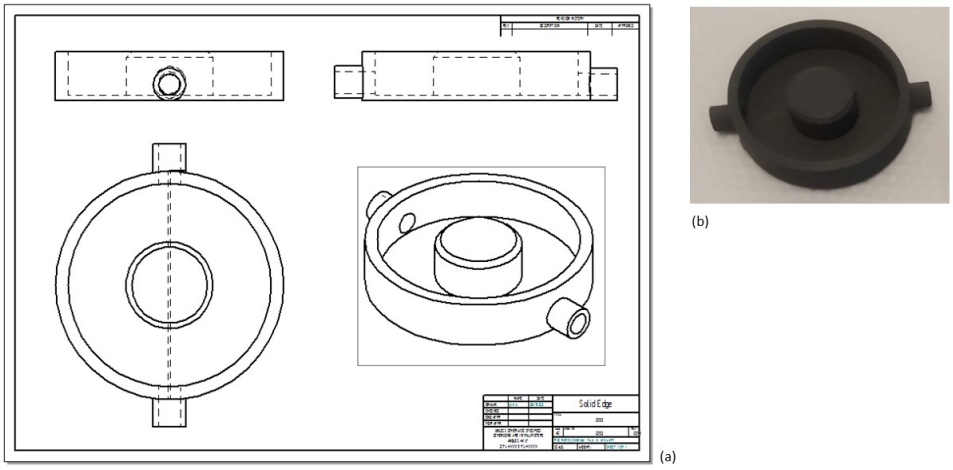

Figure 2.14: 3D chamber of Though PLA; (a) SolidEdge design paper, all spatial view; (b) Printed chamber;

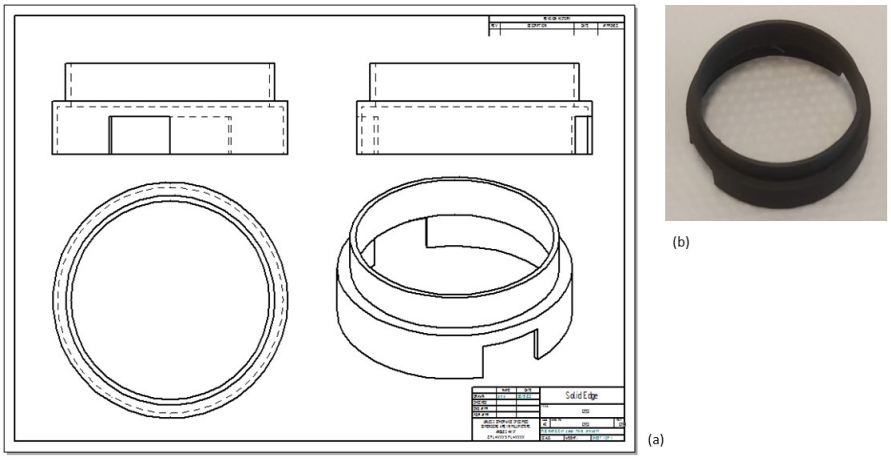

Figure 2.15: 3D chamber of Though PLA; (a) SolidEdge design paper, all spatial view; (b) Printed external wall;

would be a completely transparent dish, that would allow also reverse imaging with the microscope. However, with PLA is not possible to have good and completely transparent material.
Mainly there were three different possibilities: opaque, white, and black. The final choice was black. This is due to the fact that the opaque one is not a real transparent and the autofluorescence could be too strong and create a huge noisy background. The white one, on the other hand, reflects most of the signal but could create scattering and distorted luminous signal, creating also in this case noisy and low-quality image, hiding the signal of the fluorescent dye.

The black one was, so, the best solution, due to the low autofluorescence (it was reabsorbed by itself) and the fact that absorbs most of the impinging signal. One of the drawbacks could be the heating process, but in this case, it should not affect the cells, also taking into account that the best environment for them is around 37°C.

2.3.2 Process and assembly

The process for the assembly was based also on a practical approach. To have a reliable device several attempts were made, to arrive at a precise method that assures an efficient and reliable device. Obviously, the first step is the preparation of the three main components: bottom chamber, external wall, and silicone-rubber membrane.

- 3D printing of the bottom chamber and of the external wall, with black Though PLA as chosen material;
- cut off the membrane with the designed shape with a Silhouette blade cutter;

Then, the next step was the bonding and assembly of them. In this case, several possibilities were taken into account.
Firstly the oxygen activation plasma was tried. This should activate the group on the surface of the silicone-rubber and PLA. It should leave silanol (SiOH) groups on the surface, rendering the surface more hydrophilic and increasing surface wettability. Then, placing in contact with another oxidized surface a Si-O-Si bond should be formed. However, no stable results were reached, even if some attempts on the optimization of power and time were executed, but no big expectations were on this method.
Then PSA tape was used, which is a biocompatible and double tape, widely used on bio applications, guaranteeing good stability and adhesion.
However, some problems of leakage were observed when liquid was inserted into the dish.
So, finally, PDMS as glue was added, especially to bond the silicone membrane and the wall.
The best-defined method was, in the end, to use PSA tape to bond the chamber and the membrane. While for the bonding of the membrane with the wall PDMS was chosen.
The PDMS was synthesized by mixing 1:10 PDMS and its curing agent (the PDMS type was Sylgard 184). Then it was degassed for 30 min.

The overall assembly process was so defined by:

- Place a PSA tape, cut with the same shape of the bottom chamber edge (circular, with a width of 2 mm) on top of the chamber, and then place the silicone-rubber membrane on it, to make the adhesion;
- Distribute with a brush the PDMS on the internal surface of the wall, where there will be contact with the membrane and with the chamber;
- Insert the wall, to cover and seal the chamber + the silicone-rubber membrane;

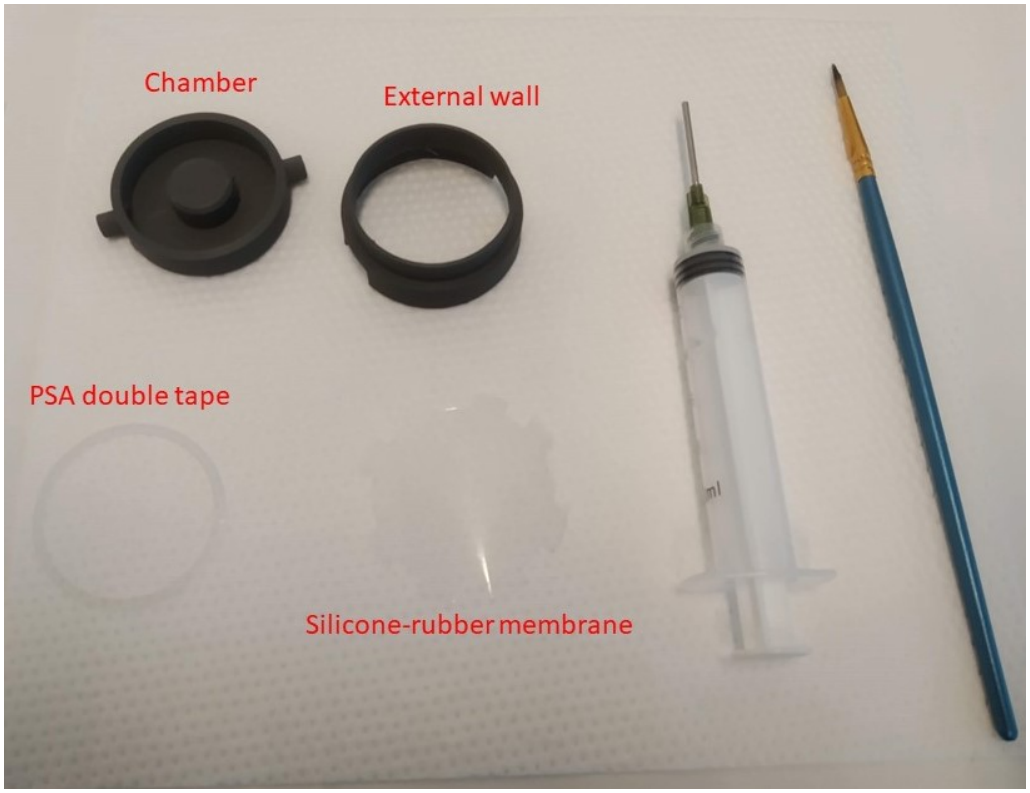

Figure 2.16: Main part and components for the final assembly

- with a syringe, distribute and pour the PDMS on the bottom of the chamber, where is the spacing between the chamber itself and the wall, to be sure that the inner part of the chamber and of the dish are completely isolated;

In this process, the use of PDMS and PSA tape assure that there is no leakage of the liquid in which cells are, but also good isolation for the application of negative pressure, providing a hermetic enclosure of the chamber.
After this assembly process and the distribution of the PDMS, the platform needs to be cured for 4h at 65°C (this temperature was chosen due to limit the thermal expansion and consequently the deformation of PLA).

Before the bonding steps, all the components were subjected to an Alconox solution bath, which is a commercial powder detergent for critical cleaning applications. Then all the parts were cleaned with Isopropyl alcohol (IPA). This process was to assure a good cleaning and first sterilization of the device, even if the sterilization process need to be completed and terminated before the cell culture was started.

2.4 Characterization

After the steps of fabrication and assembly, the device needs to be characterized, to check the real behavior of the platform and see if the radial strain is the same as the expected one.
This step goes through the use of the Digital Image Correlation algorithm, that

with image processing allows computing and extracting the strain on a region under study. This analysis is performed by the development of a simple experimental setup, composed of a Dino microscope for image acquisition and an AF1 ElveFlow Microfluidic pressure pump, controlled by PC. Then the images were analyzed by a Matlab code (Image Processing Toolbox is needed) and with the use of a support open-source software NCorr. This phase lets to check and extract the radial strain on the membrane and verify the real relationship between the applied pressure and the radial strain generated on the surface.
Other simple types of tests were performed to fully validate the platform before the biological study with HEK293T culture. Checking the absent leakages from the dish, both without pressure and with applied pressure (static and dynamic conditions), was one of the main points to validate, in other words, verify the good isolation and enclosure of the platform itself.

Overall good results are extrapolated. The device behavior is quite close to the expected one, but also the percentage of working and reliable devices over the total number of fabricated ones is quite high, validating, thus, the assembly process and the reliability of the structure.

2.4.1 Digital Image Correlation Algorithm

To correctly characterize the strain distribution on the membrane, a setup based on the Digital Image Correlation technique was implemented. The target of the DIC algorithm is to detect and extract the elongation and the strain on a material when a certain deformation is applied [21]. This technique is widely used and well-known, especially because can be easily implemented by software and can be applied to a large range of dimensions. This kind of analysis is basically independent of the dimension of the region under analysis and from the range of displacement, varying from nano/micro scale to much bigger dimensions[22]. Thus, this non-contact [23], robust and accurate technique should be the best choice to execute and extract this kind of analysis.
The basic concept behind Digital Image Correlation is to track the relative displacement of points on a surface, between a reference image, without any deformation, and a current one, in which a deformation/strain is applied. Thus, the idea is somehow to have a correspondence between points of these images, taking subsections of the analyzed images and placing and correlating the location in the current image, to finally extrapolate the displacement and consequently the strain.

The development of this algorithm is to divide the reference image into smaller sections, called subsets. The deformed subsets are then tracked in the current image with the assumption that the deformation is uniform within each subset. The reference to the current configuration transformation of the coordinates of these locations is described by [24]:

$$\tilde{x}_{cur_i} = x_{ref_i} + u_{rc} + \frac{\partial u}{\partial x_{rc}}\left(x_{ref_i} - x_{ref_c}\right) + \frac{\partial u}{\partial y_{rc}}\left(y_{ref_j} - y_{ref_c}\right) \tag{2.10}$$

$$\tilde{y}_{cur_i} = y_{ref_i} + v_{rc} + \frac{\partial v}{\partial x_{rc}}\left(x_{ref_i} - x_{ref_c}\right) + \frac{\partial v}{\partial y_{rc}}\left(y_{ref_j} - y_{ref_c}\right) \tag{2.11}$$

Here, x_{ref_c} and y_{ref_c} are the coordinates of the center of the initial reference subset, $\tilde{x_{cur_i}}$ and $\tilde{y_{cur_i}}$ are the coordinates of a current subset point, and x_{ref_i} and y_{ref_j} are the x and y coordinates of an initial reference subset point. The displacements u and v and their derivatives, all of which are constant for a certain subset, are used to parameterize the deformation. While i and j describe the relative location from the center of the considered subset. All the set of points in this subset is called S, $(i, j)\,\epsilon S$.
However, to really find and estimate the deflection from the current and reference image a correlation function should be defined, that describes correlation criteria between the setpoints. The correlation criteria defined y the DIC is:

$$C_{cc} = \frac{\sum_{(i,j)\in S}\left(f\left(\tilde{x}_{ref_i}, \tilde{y}_{ref_j}\right) - f_m\right)\left(g\left(\tilde{x}_{cur_i}, \tilde{y}_{cur_j}\right) - g_m\right)}{\sqrt{\sum_{(i,j)\in S}\left[f\left(\tilde{x}_{ref_i}, \tilde{y}_{ref_j}\right) - f_m\right]^2 \sum_{(i,j)\in S}\left[g\left(\tilde{x}_{cur_i}, \tilde{y}_{cur_j}\right) - g_m\right]^2}} \tag{2.12}$$

Where f and g are the reference and current grayscale intensity functions in a specific location *(x,y)*. On the other hand, f_m andg_m are the mean grayscale values of the reference and current subsets. The definition of these criteria is the base of the development of the DIC technique, to correlate the location in the images and extrapolate the displacement between them.
Then, several tools were developed in time, to make the easier implementation of this algorithm. In particular, for the current study, the open-source tool NCorr [24] was chosen and used, to extract the x and y displacement.

2.4.2 Experimental setup for images analysis

To develop and actuate the Digital Image Correlation technique a straightforward setup needs to be constructed. The setup has to allow the application of the pressure on the sample and in parallel acquire an image on top of the membrane.
On the surface, a marker should be randomly placed. For white platform, a black powder was chosen, while for black samples a white one was the optimal solution.
The pressure was actuated by an AF1 MicroFluidic Pump (by Elveflow). In the first version of the setup a Digital Canon camera was used, but then it was substituted by a Dino microscope, both for a higher resolution but also for higher controllability of the image acquisition. In such a way, both the microscope and the pump could be directly controlled by a laptop, which can so manage in easier and faster way the vacuum application and images acquisition. Fig 2.17 show briefly how the setup is made.

Thus, the sample was fixed by double tape under the microscope (or under the camera). A lamp was used to have a better and more uniform illumination over the sample, and to enhance the contrast between the substrate and the marker on top of it. Then, with the PC control station, the pump was actuated and the images were acquired.

A first image, without any pressure applied, was taken as a reference. Then a series of images with different pressure is acquired in series.
About the software part of the setup Fig 2.17 shows the principal steps for the image processing and strain computation. The main used tools are NCorr and Matlab.

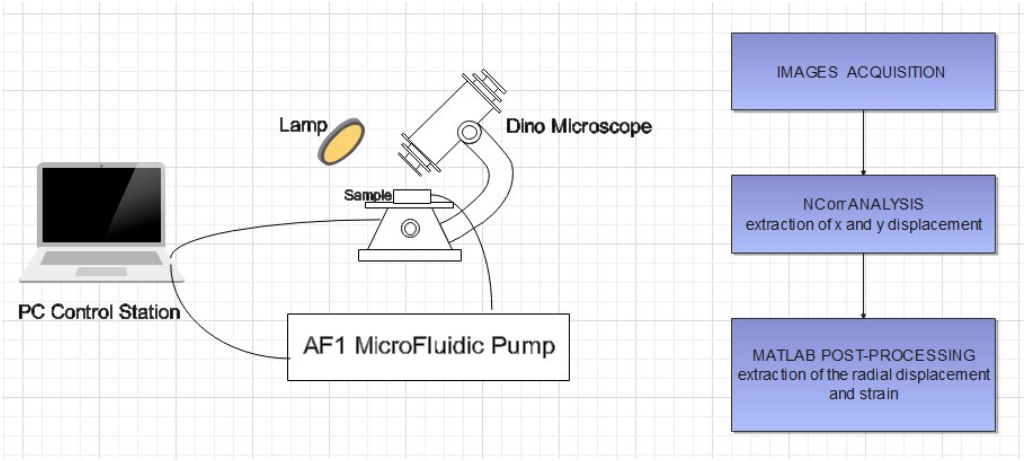

Figure 2.17: Schematic presentation of the image acquisition setup (hardware and software)

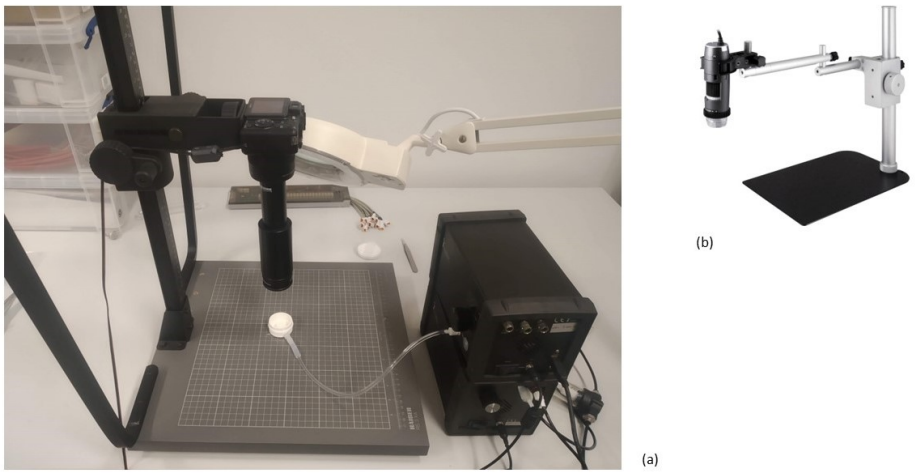

Figure 2.18: Setup implementation, sample with one inlet and AF1 ElveFlow MicroFluidic Pump: (a) First version of the implementation with Canon Camera; (b) Dino Microscope, used in the second version, for higher resolution and better controllability

With NCorr, open-source software for DIC analysis based on the Image Processing ToolBox of Matlab, it is possible to set the displacement extrapolation on a specific region of the images. The first step was, thus, to set the Region Of Interest (ROI), which corresponds to the top surface of the pillar.
Then a series of parameters needed to be set, to have a high-quality analysis and to fix the best correlation between images.
From this first step, the x and y displacements could be extracted. Then with a hand-made Matlab code, post-processing was possible from these values and the starting photos, to get the radial displacement and the radial strain. The analysis was then executed only on the ROI, which was the top of the pillar. With the code, the center of the pillar was found and from the combination of the x and y displacements, the radial displacement could be easily computed. Then, from these

values, the radial strain can be extracted, knowing the center of the pillar and the displacement of each section on the surface. For each point of the ROI, the radial distance was computed and the radial strain can be simply extracted as the ratio between the radial displacement and the radial distance.
Thus, for each pressure applied, this procedure brings to extrapolate, for each point (pixel) on top of the pillar:

- the radial displacement, that should linearly increase from the center to the edge of the pillar;
- the radial strain, which should be as constant as possible over the ROI surface;

2.4.3 Digital Image Correlation results

After the definition of the characterization setup, the data are extracted and examined. The first data came from NCorr tool, and show the vertical and horizontal displacement on top of the pillar. Fig. 2.19 shows which kind of plot comes from this study. In the figure, a 70 kPa pressure is applied on a device with a membrane thickness of 300 μm.

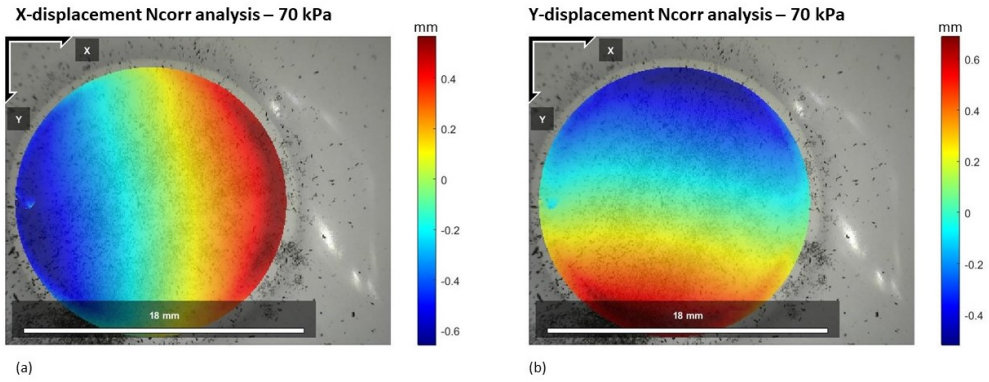

Figure 2.19: Ncorr analysis results of displacement with applied pressure of 70 kPa; (a) x-direction displacement; (b) y-direction displacement;

Then from the dataset extracted from NCorr, with post-processing on Matlab, it was possible to compute the radial strain and radial displacement on the ROI.

In particular, some interesting points emerge:

- the radial displacement increment from the center to the edge of the pillar, creating a concentric distribution of the values, as visible from Fig2.20(a). This behavior is as expected and extracted from Comsol simulation;
- the radial displacement has, more or less, a linear increment from the center to the edge, as appears from Fig2.20.(b)
- the radial strain is quite uniform on the surface, however, it is not perfectly constant. This could be due also to some error and noise in the data analysis of the image, which brings a not perfectly flat surface.

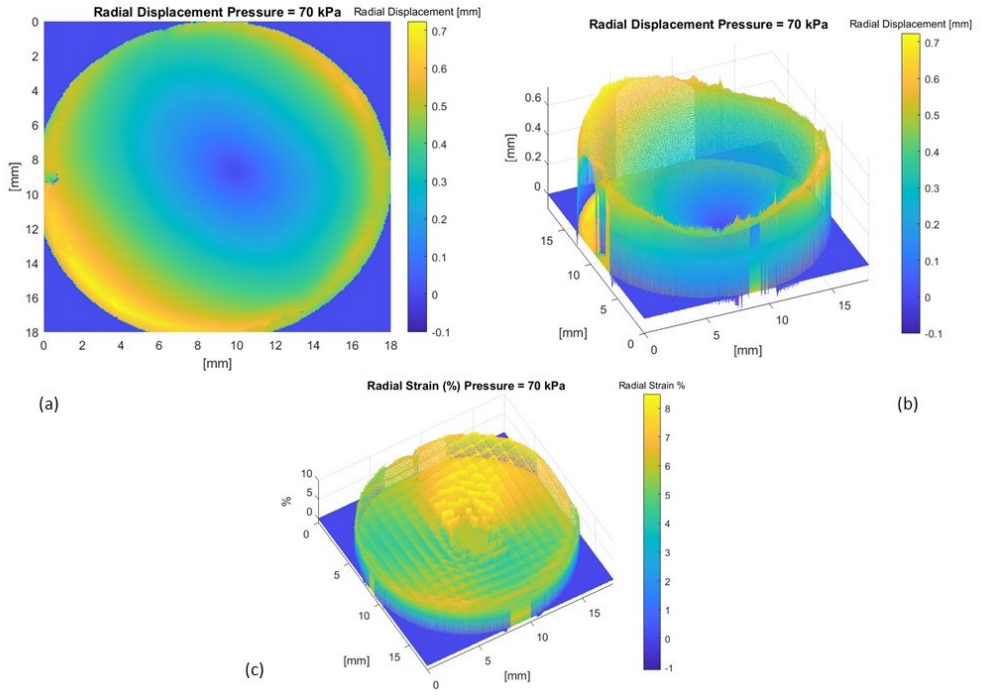

Figure 2.20: Matlab data from device with membrane thickness 300 μm at a pressure of 70 kPa; (a) 2D visualization of the radial displacement; (b) 3D visualization of the radial displacement; (c) 3D visualization of the radial strain;

Anyway, for both thicknesses, the radial strain was computed for different pressure. Through this analysis was possible to plot how the radial strain change as a function of the applied pressure on the real device.

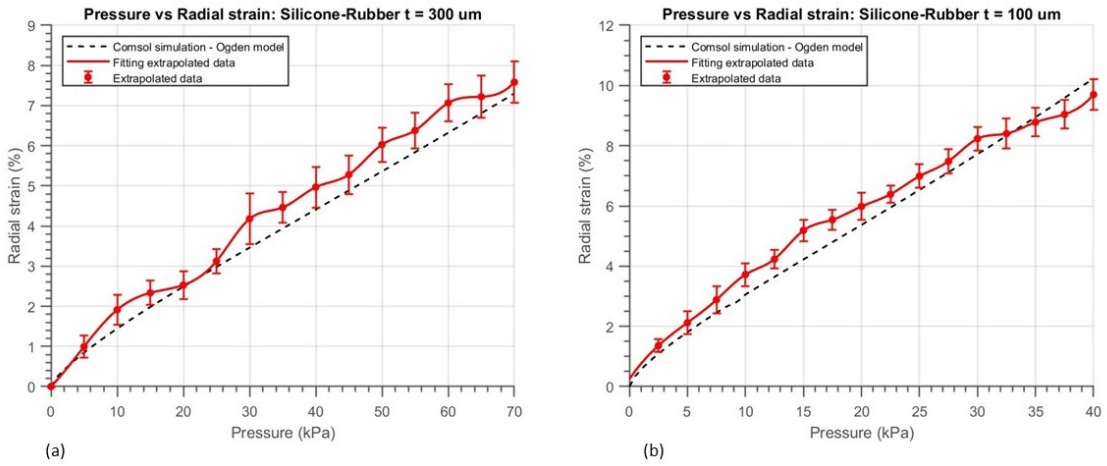

Figure 2.21: Pressure vs radial strain relation from image analysis characterization; (a) Membrane thickness 300 μm; (b) Membrane thickness 100 μm

Overall the characterized devices have a behavior quite close to the expected and simulated one. The plot show also the standard deviation of the radial strain value

on top of the surface. This value provides an idea of how much it is uniform on the ROI.

Moreover, other kinds of tests are executed, to completely characterize and validate the structure. In particular, due to the fact that for NPCs the kind of study needs to be long, so the strain should be applied for 12h/24h, the structure was tested also in the long-term. In particular, a pressure of 70 kPa was applied device with a thickness of 0.3 mm (and 40 kPa for 0.1 mm). Two kinds of studies were made. In one case the pressure was kept for 24h, in a static way, and periodically images are taken (after 1h, 6h, 12h, and 24h), to see how the strain changed in time. In the second kind of test, the pressure was applied in a dynamic way, so a sinusoidal wave with a frequency of 0.1 Hz was applied (the frequency was chosen from literature, in a dynamic study on neural cells this is a common strain rate). Also in this case, with the range of time, images are taken to check the strain variation.

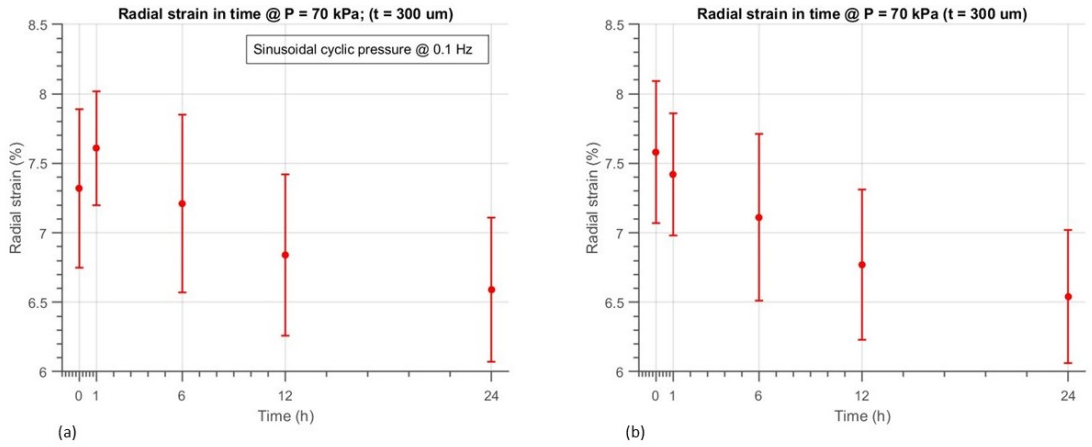

Figure 2.22: Vareition of strain in time with static and dynamic pressure applied (70 kPa); (a) Static condition; (b) Dynamic condition with sinusoidal wave;

In both cases, a decrement emerges, probably due to sliding of the membrane and bonding that decreases in time, without, however, changing in a considerable way the initial strain.

Finally, also a leakage test needs to be performed. The dish was filled with water, to check that no leakage is present. This was also tested with pressure applied, to check that the impermeability and the bond on the structure can resist also the membrane deflection. Thus, after that the assembly process was ultimate and well defined, 11 devices were built. However, 3 of them did not pass the test, while 8 are correctly working (half of them with a membrane thickness of 100 μm, and the remaining with the thicker one.)

Then the pressures to have a well-specific strain were applied, to check how far the real behavior was from the simulated one, and also to extract the standard deviation from these devices.

The main responses are summarized in Fig.2.23.

Overall the results are quite good and in line with the expectation, and, especially, the devices are quite reliable. The uniformity on the surface is the only result that

Pressure (kPa)	Expected Strain (%)	Experimental strain (%)
15	2	2.45 ± 0.30
36	4	4.78 ± 0.24
57	6	6.70 ± 0.31

(a)

Pressure (kPa)	Expected Strain (%)	Image analysis strain (%)
5.5	2	2.37 ± 0.38
31	8	8.45 ± 0.28
39	10	9.37 ± 0.32

(b)

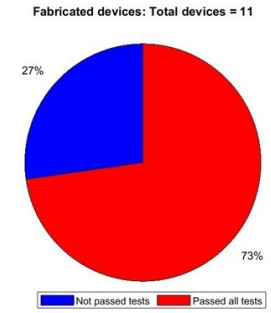

(c)

Figure 2.23: Values of images characterization on the devices that passed all the tests; (a) Table for thicker membrane, simulated and experimental behavior with pressure to have 2%, 4% and 6%; (b) Table for thinner membrane, simulated and experimental behavior with pressure to have 2%, 8% and 10%; (c) Pie graph of device that passed all the tests

does not correspond to the theoretical value, but probably this difference is especially due to the image processing and data computation on the DIC technique.
The next and final steps would be to validate from a biological point of view the device, by cells culture on it, and study the response and the morphology variation on them with a strain applied.

2.5 Mechanobiology analysis

To have a platform that allows conducting studies on the mechanobiological properties of cells, the device still needs to be validated from a biological point of view.
As a first application HEK293T culture is grown on it. Mainly, the aspects to focus on are:

- biocompatibility of the structure: check that cells survive and proliferate on it, guaranteeing a precise and effective sterilization method;
- adhesion of the cells on the membrane: for its nature cells do not adhere to silicone rubber, so it is important to verify and assure an adhesion with a proper layer;
- check the application of the strain, so the variation in the area of the cells and on their morphology;

These studies are conducted by the use of an extremely powerful tool, namely "Octoscope", from the Daan Brinks group, of Image Physics. This microscope is commonly used for voltage imaging, by the use of GEVIs (Genetically Encoded Voltage Indicators).

2.5.1 Octoscope

The "Octoscope" is a powerful tool, for optical electrophysiology, that can operate in both 1-photo and 2-photon voltage imaging and in both upright and inverted configuration [25]. A unique method for investigating neural dynamics is voltage imaging, which enables the viewing of cellular electrical dynamics by translating variations in cell membrane voltage into variations in the fluorescence of a molecular probe inserted in the cell membrane. In the case of the Octoscope, GEVIs (genetically encoded voltage indicators) are commonly used, which are engineered proteins. Eight optical stimulation and imaging configuration are possible, due to: two illumination paths, two detection pathways, and two imaging configurations (upright and inverted). This adaptability is made possible by a beam combiner that was specifically created.

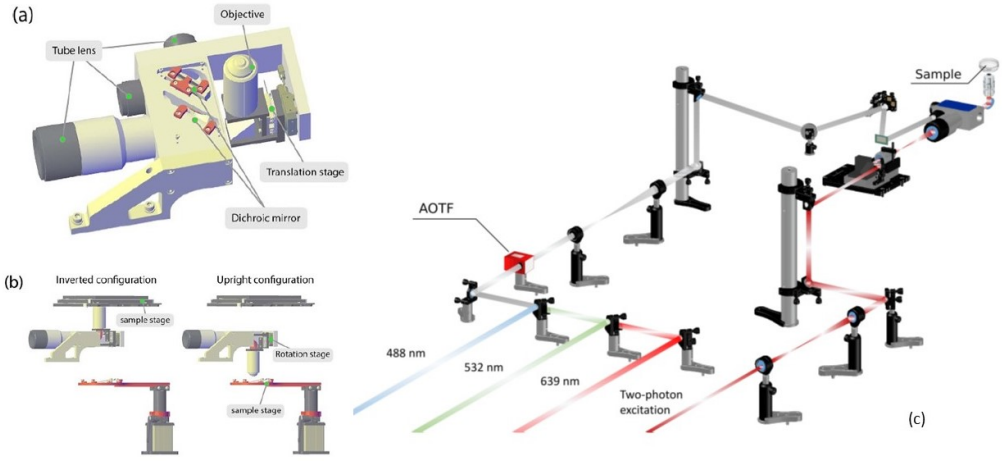

Figure 2.24: Schematics representation of the Octoscope; (a) Customized beam combined block [25]; (b) Schematics inverted and upright configuration [25]; (c) Excitation pathway of the imaging setup;

In the analysis performed, the microscope was used in an upright configuration, and with the classical 1-photon excitation. Moreover, the only light needed for the detection is the blue one (488 nm). For the study on HEK293T, GEVIs can not be used, because not neural cells. Thus, a classical differential dye for fluorescence is selected. FluoVolt Membrane Potential Dye is a fast-response probe with a potential-dependent fluorescence response. The detection is fast, allowing also to follow and analyze rapid transient, and can be used, so, for imaging electrical activity.

2.5.2 Cells culture and protocols

To develop such a kind of biological study, some protocols needed to be defined, and also some issues needed to be solved. In particular, the main points and aspects of these cells culture with the developed and designed platform are:

- find and define the best sterilization method for the platform; it has to assure the biocompatibility and be compatible with the PLA;

- find the best adhesion layer for the membrane; naturally, the cells will not adhere to it, due to the hydrophobicity and microscopic roughness, so an adhesion layer needs to be used, and verified;
- defines the protocols for the cells culture and then cells analysis
- follow the protocols to correctly use the fluorescent dye;

Starting from sterilization, PLA is a biocompatible material also used for biological studies. Nevertheless, one of the main aspects to take into account is its degradation, which could affect the organoids. For this reason a better study of the possible sterilization techniques needed to be done. In particular, [26] describe and summarize in a detailed way all the possible solutions and the future effect on the device.

Method	Technique	Advantages	Disadvantages
Heat	Dry heat/steam	Nontoxic residues, low cost, simple, fast, effective, good penetration	Not suitable for heat-and/or moisture-sensitive materials like biodegradable polymers
Chemical	Ethylene oxide	Low-temperature setting for heat-and/or moisture-sensitive materials, effective, good penetration	Potential hazards to staff and patients Toxic, flammable, and carcinogenic Long treatment/aeration time needed
	Peracetic acid	Low temperature, no activation required, odour or irritation not significant	Materials compatibility concerns, limited clinical use (only for immersible instruments/materials), no long-term sterile storage possible
Irradiation	Gamma irradiation	Nontoxic residues, low temperature, good penetration	Damaging polymers and biological materials High cost
	E-beam	Nontoxic residues, low temperature, short treatment time	Damaging polymers and biological materials, limited penetration distance
Plasma	H_2O_2 gas plasma	Nontoxic residues, low temperature setting suitable for heat-and/or moisture-sensitive materials	Not suitable for cellulose (paper), linens and liquids, and devices with hollows May cause changes in chemical and mechanical properties of polymers, produce reactive residuals

Figure 2.25: Summary table with different sterilization techniques for PLA, with advantages and drawbacks [26]

Taking also into account the possible techniques at Brinks Lab, the developed procedure was to execute a pre-cleaning, during the assembling process with Alconox solution and IPA and then, just before starting the cell culture, clean the platform with a 70% ethanol solution, that naturally evaporates (and eventually clean it with PBS to fully remove the ethanol).
This simple procedure should not affect in a considerable way the degradation of the material, but guarantee a healthy environment for the cells.

Another main aspect to take into account is the adhesion of cells on the substrate. This adhesion should be, however, sufficiently strong to allow the cells to follow the applied radial strain.
Already, from the characteristics of the material (soft silicone) extremely low adhesion, is expected, but many adhesion layers are possible. Mainly the most common solutions are [27] : plasma treatment (but low duration), fibronectin, collagen, poly-l-lysine.
On many many similar applications, [8] (especially with PDMS) fibronectin is used, showing the best adhesion properties and without affecting the mechanical properties of the system [28]. For this reason, also in this case, a fibronectin layer is chosen and placed on the membrane, showing great results in cells' adhesion to the silicone layer.

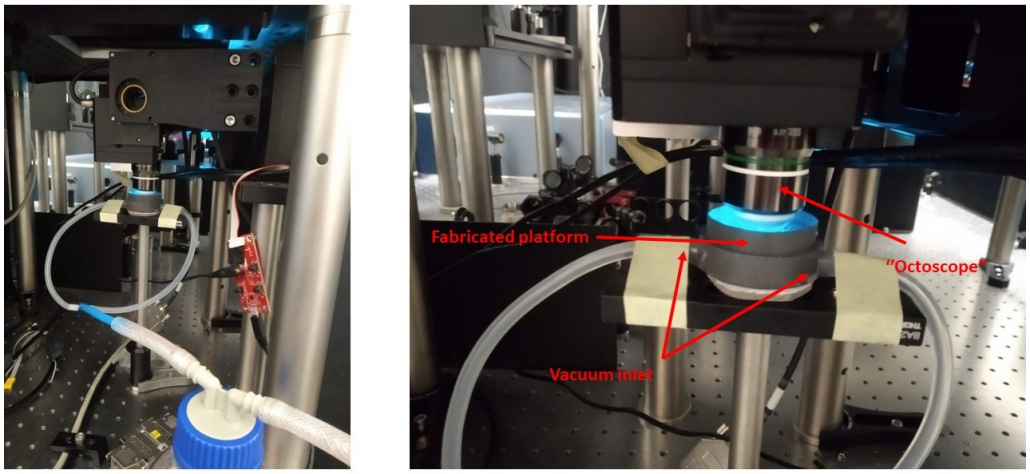

Figure 2.26: Fabricated platform with HEK293T culture, under study with "Octoscope";

Finally, the cell culture is started on the made platform. After the duplication they are placed on the dish, with 3 mL of medium, to fully cover the surface. The cells under study are HEK293T, which are tumoral human embryonic kidney cells, so immortal. The usual diameter of this type of cell is around 20/30 μm. Then, after that, they are placed on the dish, and the characterization is done after 24h, otherwise, the membrane became overcrowded. The medium is then removed, and the plate is washed three times with a physiological buffer. The FlouVolt solution is then added and incubated for 30 min. Finally, the medium is again removed and 3 mL of the physiological buffer is added for the microscope analysis. Fig 2.26 shows the fabricated device with HEK293T cell culture under analysis at the Octoscope.

2.5.3 Results

Finally, cell cultures are started on the devices. As a biological specimen, HEK293T is chosen, due to the fact that are quite common and standard cells, robust, and with a diameter around 10/20 μm, thus, having the Octscope a resolution of 233 nm, should be quite easy to detect the variation in the shape and in the area.
The main target of the biological validation was to check and verify the biocompatibility of the system and the application of the strain on the cells.
some first tests are done without any adhesion layer, and, as expected, the adhesion was very low.

What was done, for different devices, was to place in a location on top of the pillar and apply a sweep in the pressure, so several images with many pressures are acquired. This process was done for different locations on top of the pillar to have better statistics and more analysis.
From each image, through the use of ImageJ (a free software widely used for biological specimen analysis), it was possible to extract the area of the cells for different pressure. As already introduced the area should change (approximately) by a factor $(1 + \varepsilon_{r,r})^2$. Thus, delimiting the sharp edge of cells, it was possible to compute the

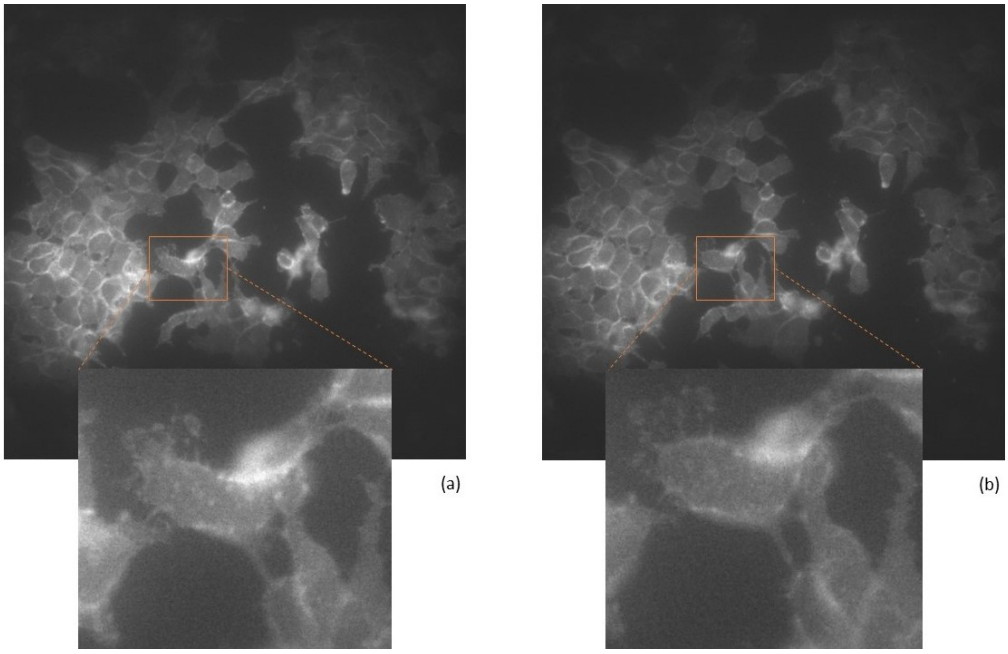

Figure 2.27: Miscroscope image on device, with no stretch and expected 10% strain (500m x 500m); (a) No strain applied; (b) Applied pressure equal to 40 kPa, expected strain 10 %;

area (for no strain and different pressure) and extract the strain. It is important to highlight how the images are taken in different locations on the pillar to have more accurate data and to check the uniformity. Moreover, it has to be kept in mind that this process is affected by a small intrinsic error due to the limit in resolution when the cells are delimited and the area computed. In some cases, the luminosity of the edge is smoother and the contrast lower, introducing a basic small error in the area computation (due to the number of pixels taken into account). Nevertheless, this study is extremely important to validate the biocompatibility of the platform and check the real transmission of the strain to the cells.
Fig2.27 show an example of a non-stretched and stretched cell, on a device with a membrane thickness of 100 μm, where the zoom show the change in shape and area.

All eight devices are tested. Firstly on two devices cells are plated and checked with a classical microscope just to check the survival of the cells. Two devices are used without any adhesion layer, to really check if it was needed, and finally, on all the remaining four (2 with 0.3 mm membrane thickness and 2 with 0.1 mm thickness) a complete characterization was executed, with the use of fibronectin as an adhesion layer.
The first important result is that on all the devices cells survive, giving a biocompatibility rate of 100%.
Then, the main results about the strain are reported in Fig 2.28 and Fig 2.29.

About the device with a membrane thickness of 0.1 mm, Fig 2.28.(a) shows how the experimental strain (extracted as the average of the computed strain in different locations of the pillar) is lower than the expected one. In particular pressure of 31

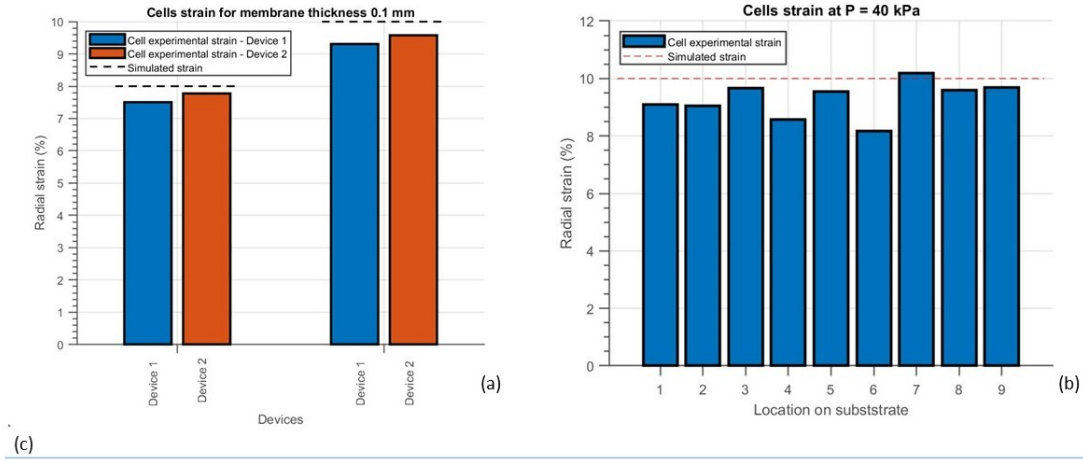

(c)

Expected Strain (%)	DIC strain (%)	Experimental cells strain (%) – Device 1	Experimental cells strain (%) – Device 2
8	8.45	7.51 ± 0.43	7.78 ± 0.37
10	9.37	9.31 ± 0.62	9.57 ± 0.51

Figure 2.28: Summary of devices characterization with 0.1 mm membrane thickness; (a) Histogram extracted strain for different pressure with expected strain 8% and 10% for two devices; (b) Extracted strain (expected 10% for one device in different location of the surface; (c) Table summary of Digital Image Correlation strain and cell experimental one;

kPa and 40 kPa are applied to have a simulated strain of 8% and 10%. Fig 2.28.(b) show for Device 1, the compute strain in different locations of the pillar when a 10% is expected. What is possible to see is that the experimental one is quite close to the theoretical but there is a considerable standard deviation, so a non-negligible variation due to the analyzed location. Finally Fig 2.28.(c) summarize these results.

Fig 2.28 shows the same time of analysis but for devices with a membrane thickness of 0.3 mm, and applied pressure of 36 kPa and 57 kPa, to have an expected strain of 4% and 6%. In this case, the experimental strain is higher than the theoretical one but closer to the strain computed with the Digital Image Correlation technique.

2.6 Discussion

Due to the necessity to have a platform that can allow mechanobiological study on neural cells (but also different biological specimens) a device that can actuate a controlled strain is developed. All the developing phases are performed, till to arrive at a validated platform also from a biological point of view.
The first steps were the design and the concept of the device, also from already existing solutions. Optimization of the hyperelastic models was also performed.

Then the fabrication and assembly process was optimized, to have a reliable and robust device, also for long-term studies. This step was executed especially in a

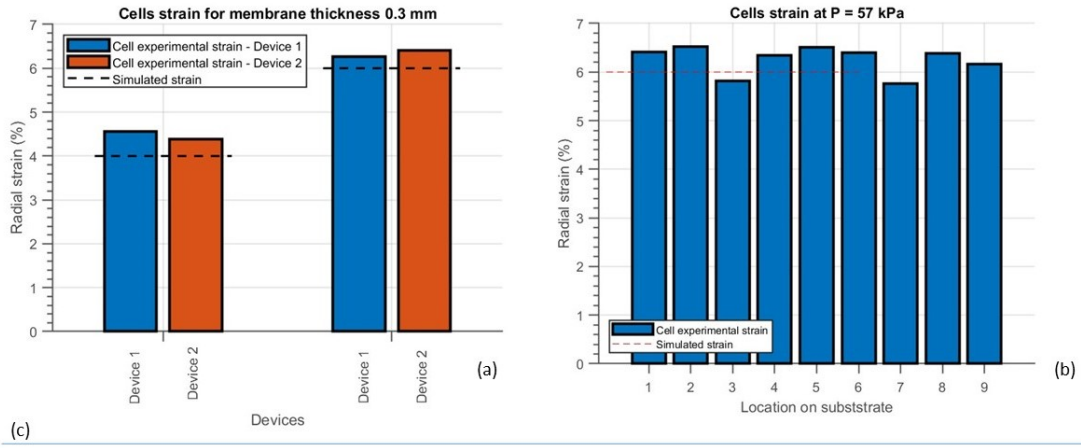

Expected Strain (%)	DIC strain (%)	Experimental cells strain (%) – Device 1	Experimental cells strain (%) – Device 2
4	4.78	4.56 ± 0.61	4.96 ± 0.64
6	6.70	6.26 ± 0.29	6.41 ± 0.33

Figure 2.29: Summary of devices characterization with 0.3 mm membrane thickness; (a) Histogram extracted strain for different pressure with expected strain 4% and 6% for two devices; (b) Extracted strain (expected 6% for one device in different location of the surface; (c) Table summary of Digital Image Correlation strain and cell experimental one;

practical approach, trying different processes and testing them. PDMS and PSA tape need to be used to guarantee a good enclosure.

A characterization step was then necessary, to verify the real behavior of the device. This analysis was executed by a Digital Image Correlation technique, through the use of a simple hand-made setup and by Matlab processing. The extracted results follow with good precision the ideal behavior, taking also into account the limitation of the image acquisition and data processing.

Finally, a biological study was conducted, to fully validate the device. HEK293T cells are used, and a morphology analysis is done. From the area variation of these cells under stress was possible to extract the real sensed strain, which also in this case followed the ideal behavior but with a non-negligible error. This study highlights the biocompatibility of the structure and its behavior, but a more detailed study needs to be conducted, to reduce the associate error, especially in terms of resolution and data acquisition.

Chapter 3

Biodegradable stretchable electrodes

3.1 Introduction

The second part of the project was about the development of biodegradable stretchable electrodes, with a capacitive structure that depends on the applied strain.

One of the main points in the final scaffold development is the integration of stretchable electrodes, made of biodegradable material, that can interface and interact with the neural system. Moreover, strain sensing mechanics need to be inserted, to monitor the applied elongation for the mechanical stimuli of the nerve.
In particular, the main targets are to set the milestones for the development of such devices, to integrate them into the scaffold. The main topic are then:

- the synthesis of different biodegradable materials as stretchable substrate (PGS, POMaC, and PGSA);
- design and development of a stretchability pattern that also allows monitoring the strain by capacitive variation;
- try and choose the most suitable microfabrication techniques with these materials (iron layer by spark ablation was finally chosen);
- develop a setup that makes it possible to stretch and, in parallel, measure the capacitance (in general the impedance);

3.1.1 Stretchable electrodes

Recent advantages both in material science and microfabrication techniques have brought a huge development in flexible electronics. In particular, the definition of flexible and stretchable electronics has a large variety of applications, especially for medical and wearable applications.
Over years, many materials and shapes are developed [29].
However, in this case, a simple and planar shape was chosen, that could be later on improved. The electrode is then made of two main components.

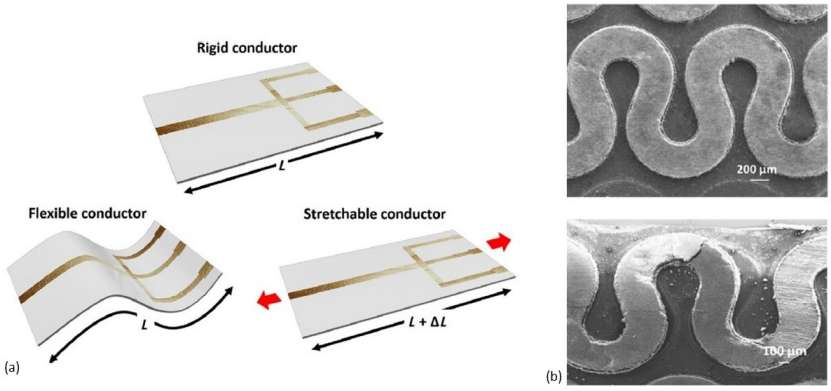

Figure 3.1: Characteristics of the wavy stretchable pattern; (a) Definition of the parameters for the geometrical wavy shape [30]; (b) Stress distribution on the pattern [31];

Firstly, a stretchable substrate is needed. It needs to be an elastomer, biocompatible and biodegradable, on top of which is possible to deposit a conductive metal pattern. The second part is the development and design of the conductive line, which characterizes the conductivity of the electrode, but also the maximum stretchability avoiding any failure. Also, in this case, many solutions were developed [32], but for the planar electrode, one of the most reliable and efficient was the serpentine shape, as shown in Fig 3.2.(b), which assures a high stretchability and low rate of failure [31].

3.1.2 Planar strain sensing

On the other hand, a strain sensing mechanism needs to be introduced. In this case, the most suitable solutions are the resistive type, capacitive type, and resonant type. This kind of structure can be easily integrated and characterized by specific conductive patterns, and with elongation, they change their characteristics.
The resistive one is based on the variation of the resistance of the conductive line with the application of a strain. Several effects could influence this behavior (tunneling effect, crack propagation, disconnection mechanism, piezoresistive effect) [33]. On the other hand, the capacitive sensing mechanism is based on the variation of the capacitance of the pattern, due to the structure geometrical deformation. Usually, this kind of sense has a higher stretchability and lower rate of failure with respect to the resistive one, that on the other hand is usually characterized by a greater sensitivity.

Fig. 3.2.(a) shows an example of an interdigitated structure for strain sensing, with the capacitive variation with respect to the applied strain [34]. While Fig. 3.2.(b) shows an spiral example of capacitive strain sensor [35].
From these examples, the construction of a capacitive sensing pattern was set and designed.

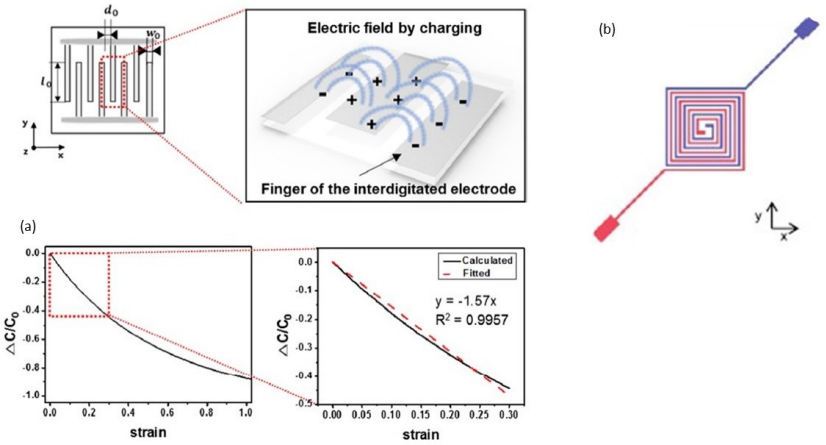

Figure 3.2: Example of capacitive strain sensor for stretchable electrode; (a) Interdigitated capacitive strain sensor, with characteristic response [34]; (b) Example of spiral capacitive strain sensor [35];

3.2 Design and methodology

The target of this part of the project was, thus, to develop stretchable electrodes that should work as a strain sensor. The strain will be detected through a variation in the capacitance on top of the substrate. Thus, mainly, the electrode will be composed of a biodegradable substrate and a metal pattern deposited on top of it.
Different parts needed to be taken into account to develop such a device. First of all, develop and synthesize a biodegradable substrate. For this reason, different materials (polymers) were synthesized and tested. The chosen solutions were: POMaC, PGS, and PGSA. While for the POMaC and PGS the synthesis process was well defined and well known, the one for the PGSA was quite long and complex to develop. Moreover, some optimization and different variations on the process were made, to have handling and stretchable substrate, that can better fit with this type of application.

Then the metal pattern on top should be chosen. The choice was on the basic wavy shape, which is well known and guarantees the best stretchability. This kind of pattern is defined by 4 different parameters: width of the metal line (W), length of the rectangle that join two arcs (L), radius of the circular arc (R), and the angle of extension of the arc (α).
Then, some specific shapes need to be introduced to maximize the capacitance variation as a function of the strain. For this, both from literature and trying to think and optimize new shapes, two main patterns were defined, simulated, and tested: interdigitated and concentric spirals.

Finally, these kinds of devices were simulated on Comsol. The aim of these simulations was to have an idea of the behavior of the electrodes, extract how the capacitance change as a function of the strain, optimize and study how the capacitance changes depending on the geometrical dimensions of the pattern, and

finally see the distribution of the electric field and electric potential, just to have a better understanding of the electrical response.

3.2.1 Stretch-ability pattern

Starting from a literature review, the most efficient and well-known pattern for the planar stretchable electrodes is the wavy one. This pattern is widely used for this type of application, because guarantee high stretchability, and also for metal layer on top of stretchable substrates. The shape is composed of an alternation of a circular arc and rectangular line. This pattern is defined by four parameters:

- W: width of the metal line;
- L: length of the rectangular shape that connects two arcs;
- R: radius of the circular arc;
- α: extension of the circular arc;

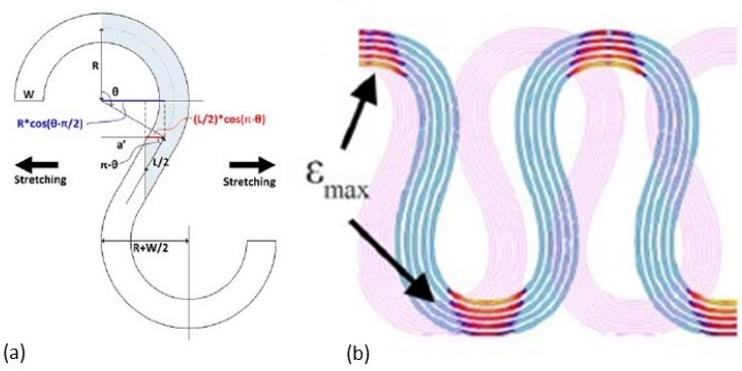

Figure 3.3: Characteristics of the wavy stretchable pattern; (a) Definition of the parameters for the geometrical wavy shape [30]; (b) Stress distribution on the pattern [31];

To have a feasible construction, some geometrical constraints are present, to guarantee that different arcs do not overlap. From a simple geometrical analysis of the structure is possible to impose that:

$$R\cos\left(\theta-\frac{\pi}{2}\right)-\frac{L}{2}\cos(\pi-\theta)\geq\frac{1}{2}\left(R+\frac{W}{2}\right) \tag{3.1}$$

$$\theta\leq\pi-\arcsin\left(\frac{1}{2}+\frac{1}{4}\frac{W}{R}\right);if\ (L=0) \tag{3.2}$$

$$\frac{L}{R}\leq 2\sec\theta\left(\frac{1}{2}+\frac{1}{4}\frac{W}{R}-\sin\theta\right);if\ (L\neq 0) \tag{3.3}$$

Ideally, the maximum strain reachable with such kind of configuration is quite high, especially compared to the expected one for the scaffold application. The critical point in such a structure is on the top of the arc, where the maximum stress is got.

In this case, some extra relationships are imposed for the design of this pattern, to limit the number of grades of freedom and to be sure that the imposed values for the parameters respect and correctly solve the geometrical conditions. In particular $W = L$, $R = \frac{3}{2}W$ and $\alpha = 110°$. These assumptions limit the variation only to W, because all the other parameters are expressed as a function of the width.

3.2.1.1 Strain sensing

As a further step, to detect and monitor the strain, a structure that is sensible to the stretch of the substrate is needed. Several solutions exist, but in this case, a capacitive strain sensor is chosen.
The main aspect became then to choose the optimal structure, that could assure a good sensitivity. Obviously, the first solution was a simple parallel plate capacitor, with a wavy shape that is divided into two lines whose edges end with two parallel vertical lines. However, this kind of solution could not give high performance. The basic capacitance itself could be improved, same for the sensitivity.
Thus other possibilities are chosen, in particular, two different structures were designed and tested: interdigitated and concentric spirals.

The interdigitated solution is quite common for this kind of sensor because increases the basic capacitance and its variation with the strain. However, the designed shape was improved from a stretchability point of view, putting a wavy shape on the long horizontal line. This kind of metal line could be easily broken and failed and can crate intern crack, decreasing in a considerable way the performance. Using, then, also in this region a wavy shape, could assure better quality and resistance in the stretching. In particular, the used shape is a trigonometric function (sen).
For the second solution, spirals were used. In particular, an Archimedean spiral can be defined by the equation:

$$r = a + b\vartheta; \tag{3.4}$$

So, using two different spirals, concentric, the capacitance can be maximized and also its sensitivity to strain. However, in this case, it is not possible to detect the direction of the strain, because it is a symmetric structure, thus there will be the same variation with strain from all directions.

Finally, three different shapes are designed and fabricated:

- basic wavy pattern: just as a reference and to check the conductivity;
- interdigitated;
- concentric spirals;

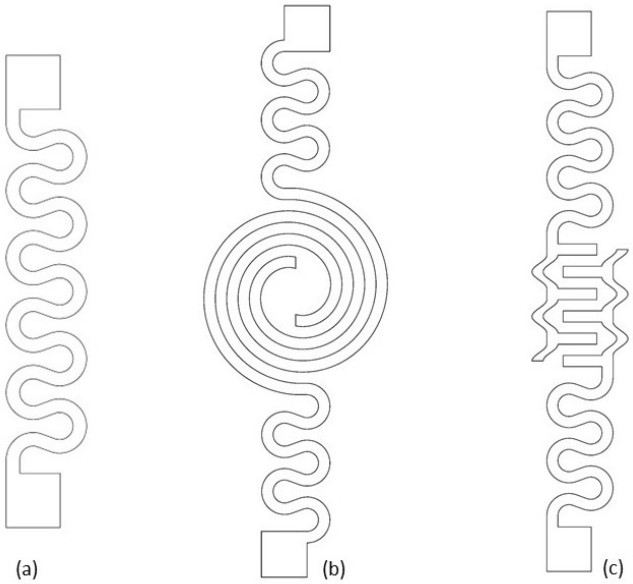

Figure 3.4: Design of the three masks; (a) Basic wavy shape; (b) Concentric spirals pattern; (c) Interdigitated wavy pattern;

3.2.2 Simulations

From these designs, Comsol simulations were executed, to extract the dependence of the capacitance to the strain, how the geometrical dimensions change the basic capacitance, and to better understand the electrical response of the electrodes. The structure itself is made mainly of two-component: the biodegradable substrate and the metal pattern on top of it.
The substrate is simply a parallelepiped, that was defined with dimensions that depend on the dimension of the pattern (width and length). The thickness was defined initially as 1 mm, which should be a reasonable value for the stretchable electrodes, making them sufficiently robust.

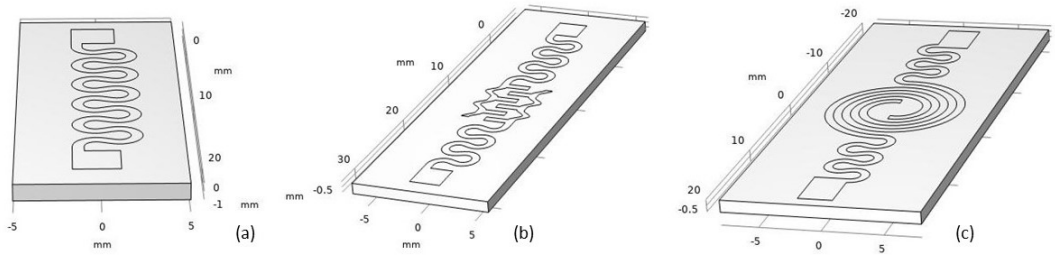

Figure 3.5: Simulated Comsol components; (a) Basic wavy shape; (b) Interdigitated wavy pattern; (c) Concentric spirals pattern;

The pattern was designed on the workplane and extruded. The thickness of the conductive layer is set to 100 nm.

All the geometrical dimensions, the design, and the characteristics of the different patterns were described in a parametric way, so easily change them and execute eventually study on their dependence.
Two physics are needed for this kind of study: solid mechanics and electrostatic.

About the boundary to set, they are quite simple. From a mechanical point of view, the bottom surface of the substrate is fixed, the same for one of the lateral faces, that was the face fixed of the electrodes. The opposite face was one in which a displacement is applied, to stretch the structure. This displacement was subject to a parametric study, to see how the capacitance and other parameters change as a function of the strain.
From an electrostatic point of view, one terminal was set as ground, while on the other one a voltage of 1 V was applied, to be able to compute the capacitance.
The boundaries to add are so quite straightforward, but what could be tricky is the definition of a good mesh to have a precise description of the electrode's behavior, especially being present components of a totally different ratio (from mm to nm).
For this reason, the mesh was defined by the use of two *Tree Triangular* mesh on the top surface of the metal pattern and the substrate. Then they are linked by a *Swept* in the mesh. Finally, for the substrate, another *Swept* is defined, with the use of the *Distribution* function.

Also, in this case, the polymeric substrate is considered hyperelastic. The parameters used in these simulations were extracted from the DMA test on a PGSA sample. An Ogden model was chosen, characterized by: $C_{10} = -0.22974MPa$ and $C_{01} = 1.2142MPa$;

3.2.3 Simulation results

From the Comsol simulations, a fisrt sweep over the width was executed, to extract how the basic capacitance change as a function of the W.
The same kind of study was done for the thickness.

Due to the fact that the other parameters are all related to the width (they need to satisfy the geometrical constraints), the capacitance increase with the width itself, and the type of curve is similar for both interdigitated and spiral. However, in the case of the spiral one, there is a bigger dependence on this value, due to the fact that increasing the width also the length of the spiral increase, providing a considerable increment in the capacitance due to two parallel lines of the concentric spirals.
On the other hand, the thickness study was performed between 100 and 500 nm, but due to the small variation the basic capacitance could be very low affected by that, and it is not subjected to considerable changes.

What is important to extract, especially, once the width and the thickness are fixed (thickness equal to 100 nm and width equal to 700 μm), is the basic capacitance and how the capacitance change with the strain. In particular, from the executed simulation, the basic capacitance of the structure are:

- Interdigitated structure: $C_0 = 0.245$ pF

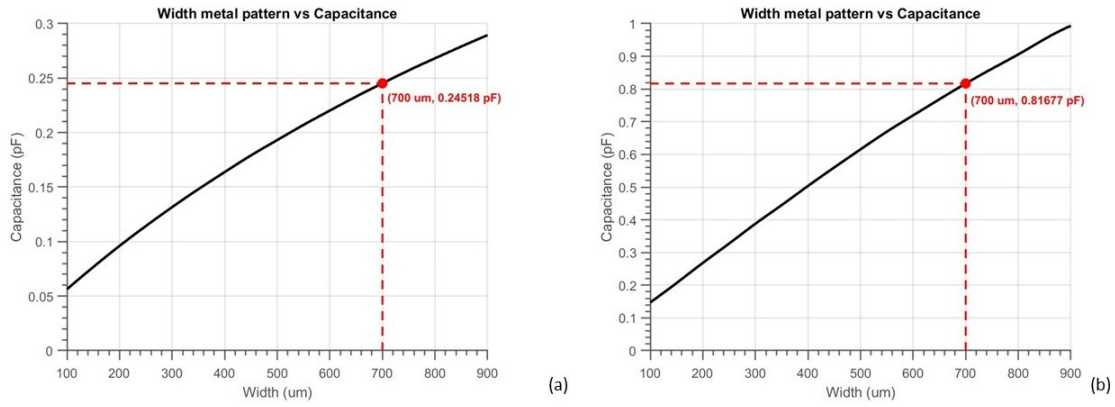

Figure 3.6: Dependance on the basic capacitance from metal width of the pattern; (a) Basic capacitance as a function of the metal width in interdigitated structure; (b) Basic capacitance as a function of the width in spiral structure

- Spirals structure: $C_0 = 0.816$ pF

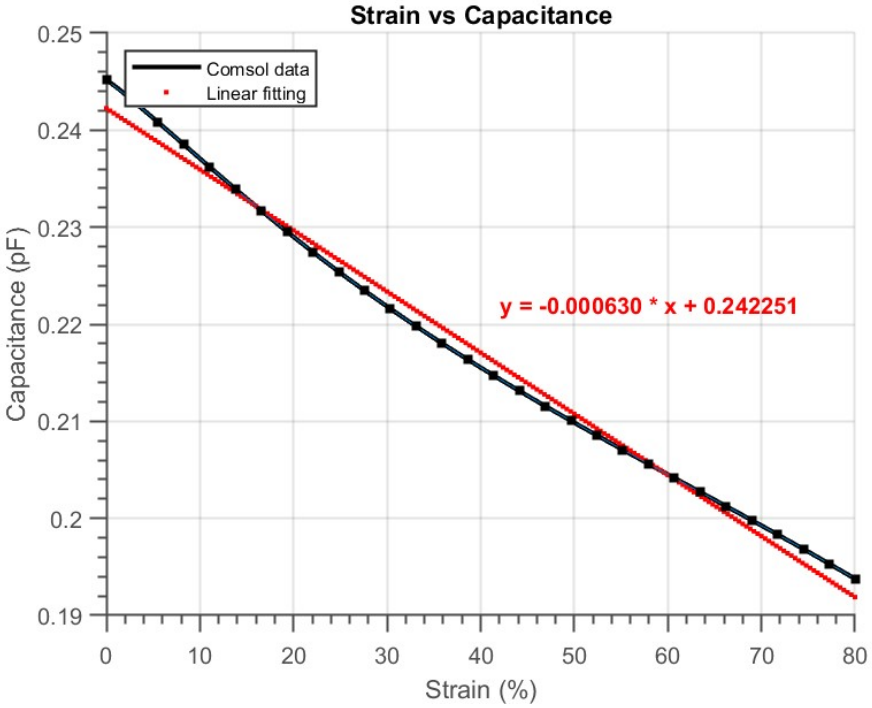

Figure 3.7: Variation of the capacitance as a function of the applied strain with the extrapolation of the best linear fitting in the interdigitated structure;

From Fig.3.7, it is possible to see how the capacitance decrease with the strain, as expected. The maximum variation, however, is in the order of tens of fF, so quite small. Moreover, the relation is not linear but can be approximated by a linear fitting shown in the plot, but due to the small variation, also the sensitivity is not very high.

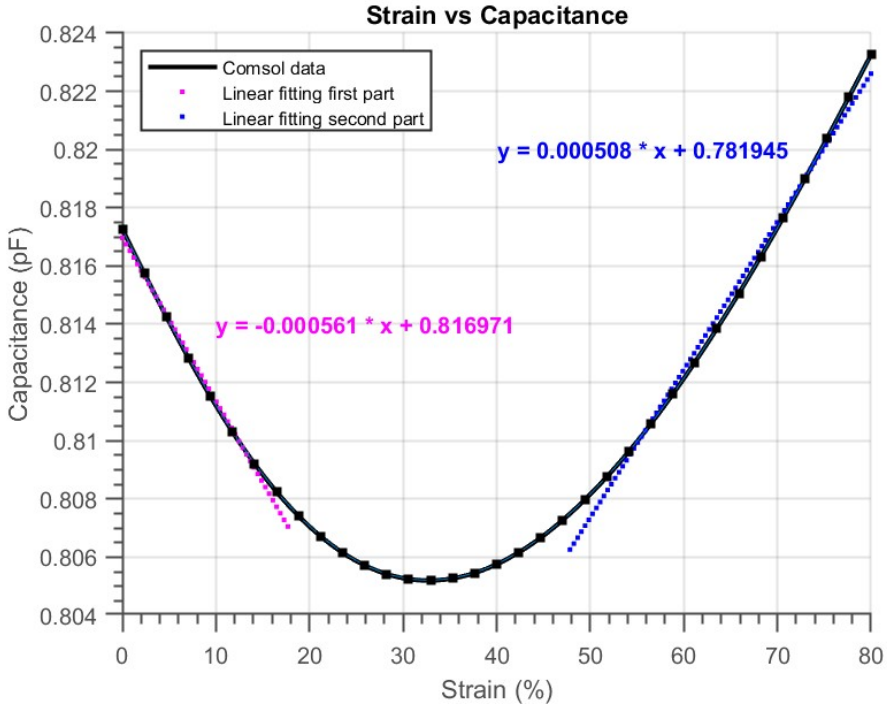

Figure 3.8: Variation of the capacitance as a function of the applied strain with the extrapolation of the best linear fitting in two different regions in the spirals structure;

Fig.3.22, on the other hand, show the behavior for the spiral one. The interesting part is that, in this case, the variation of the capacitance is not monotonic, but there is a first region in which the capacitance decreases, and then, after a minimum value, it starts to increase. This is due to the fact that, applying a strain along one direction (x-direction), in the first part reveals the increasing distance between the lines in the elongated direction, but after a certain limit, the compression along the perpendicular direction of the strain (y-direction) start to dominate, and the capacitance increases. In general, thus, is also possible to conclude that for this kind of capacitive sensor, there is a huge dependence on the elastic properties of the material, especially on the shear modulus.
However, also in this case, the capacitance variation is quite small, providing a sensitivity similar to the one of the interdigitated.
For this structure, on the other hand, the two decreasing and increasing regions, can be well-fitted by a linear approximation.

The simulation also provides information about the electric field distribution and the stress on top of the surface, which can be useful for a better understanding of the sensors themselves. In particular Fig.3.9 show the electric field distribution on the spiral structure, for not-stretched and stretched substrate. The stretched zoom on the spirals especially shows a much higher electric field along the perpendicular direction of the strain, proving why it is present as a switch in the capacitance variation.

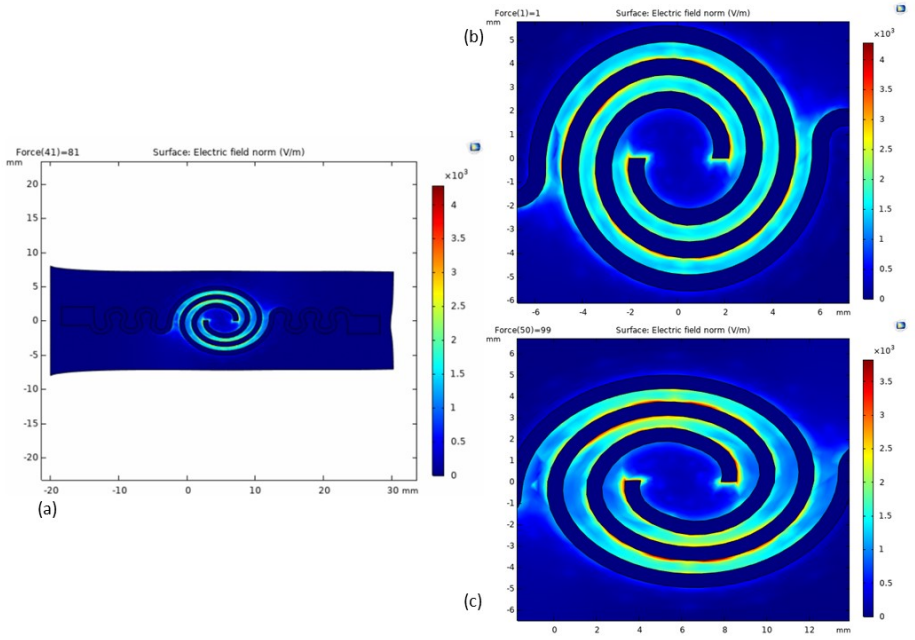

Figure 3.9: Electric field in the spiral structure from Comsol simulations; (a) Electric filed with elongated structure; (b) Zoom on the spiral for no strain; (c) Zoom on the spiral with strain applied;

3.3 Fabrication

The next step in the development of such a design was the real fabrication of the electrodes. Mainly two parts need to be developed: the polymeric substrate and the metal pattern deposited on top. The most important point was so to optimize and better develop/define the synthesis process for the different polymers (POMaC, PGS, and PGSA) and then try some deposition techniques on them. This was not so straightforward. Some of these polymers, especially PGSA, are not common, and the response and feasibility of different depositions need to be tested and verified.
What comes out is that for small samples e-beam evaporation can be executed, but with larger samples and larger thicknesses (such as 1 mm), the evaporator (but also the sputtered) can not work. The machine can not reach the minimum value of vacuum due to the degassing of the polymer, even if many times it was executed in the synthesis process. Moreover also plasma cleaning, a step needed to avoid contamination in these types of machines, in some cases affect a bit the surface of the polymers, basically etching them.
However, the best deposition was through spark ablation, which does not need a high vacuum level. Thus, in the end, the metal pattern on top was made by nanoparticle of Fe. Nevertheless, to improve the adhesion, a layer of PVA was used.

Moreover, to have some reference samples in which the metal layer was deposited by evaporation, some test samples were made using soft silicone as substrate.

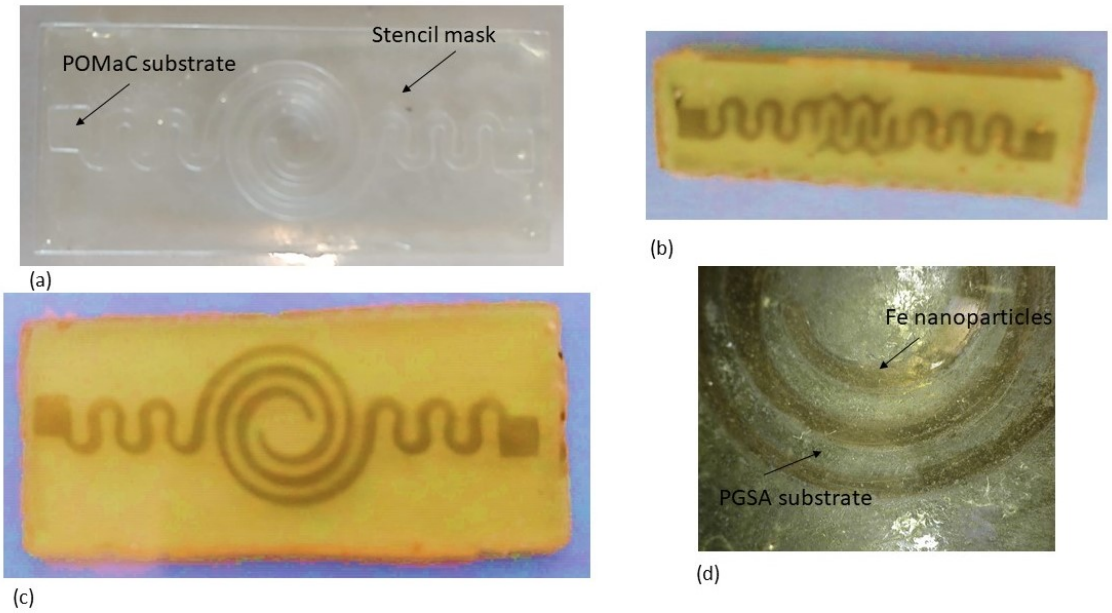

Figure 3.10: Stretchable electrodes during fabrication process; (a) POMaC substrate with stencil mask on top; (b) PGS substrate and Fe nanoparticle layer, interdigitated electrode; (c) PGS and Fe nanoparticles layer, spiral electrode; (d) Zoom by Dino Microscope on PGSA substrate with nanoparticle layer;

3.3.1 Material

About the substrate, three different polymers were synthesized and the synthesis process optimized: POMaC, PGS and PGSA. On the other hand, about the metal layer, iron was chosen due to its degradability. Mainly two techniques were possible: evaporation and spark ablation. However, for the evaporation, there were some problems due to the degassing of the polymers inside the chamber, avoiding the vacuum level needed for the deposition itself.
On the other hand, also sputtering Molibdenum was a choice, but due to the same problem about degassing it was not tested.

3.3.1.1 PGS

PGS - poly(glycerol sebacate) is a biodegradable polymer that is being used in more and more biological applications. Glycerol and sebacic acid are polycondensed to create this elastomer. The biocompatibility and biodegradability of PGS are both very important characteristics in biomedical applications [36]. This polymer is non-immunogenic, and it was proved to be non-toxic and cause only a minimal inflammation n*in vivo*. This was discovered and synthesized in 2002, and started to spread quite fastly for its mechanical properties, biodegradability, and relatively inexpensive chemicals. PGS is able to degrade and further resorb *in vivo*. Mainly two steps are present for the synthesis process: polycondensation and crossing.

The first synthesis process [38], was based on the main two steps described in Fig.3.13.

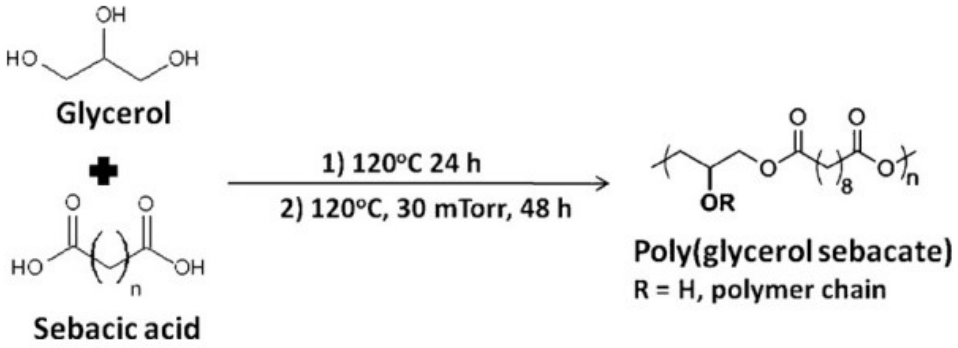

Figure 3.11: First developed PGS synthesis process [37]

However, in time, some applications and different parameters are tested, especially to change and tune the properties of the materials.
The protocol followed for the synthesis of PGS starts mixing together an equimolar amount of glycerol and sebacic acid. The solution is extremely dense and needs to be slowly mixed with a magnetic stirrer bar. This process needs to be executed at a temperature of 120° C for 2h, with a nitrogen flux always active during the polycondensation.
After that, the first main step was concluded, and the crosslinking needed to be performed. To do that the mixture was poured into a beaker, covered with aluminum foil (with some holes), and keep in a vacuum furnace for at least 22h. This process could last till 96h, depending on the cross-linking level that wants to be reached. The temperature was fixed at 120°C, but also this parameter could be changed to vary the material properties.

3.3.1.2 PGSA

PGSA (Poly Glycerol Sebacate Acrylate) is a polymer that starts from the PGS and especially was developed with the aim to overcome the thermally processing of PGS and have a photopolymerization process. The PGS prepolymer was chemically modified by introducing reactive acrylate moieties [39]. This polymer shows wide tunable properties, depending on the temperature and duration of some synthesis steps, but especially on the acrylation degree. Several chemicals are needed to correctly perform this synthesis and especially it is a quite long process, that last for several days. The overall process is described, in general, in [40] and [39]. PGSA prepolymer consists of a mixture of 10% (w/v) of PGS prepolymer, 0.05% (w/v) 4-methoxyphenol, and 0.01% (w/v) 4-(dimethylamino)pyridine in dichloromethane [40]. For the acrylation phase, an ice bath needs to be prepared. Acryloyl chloride and Triethylamine are added and mixed, for 24h, under nitrogen flux. Then a phase of post-processing and purification is needed. 4-methoxyphenyl need to be added and mixed. The mixture was placed in a flask, and the flask in a water bath at 40°C, with a vacuum of 450 mtorr. Dichloromethane will evaporate, till it left a viscous liquid inside the flask. Ethyl acetate is then mixed, to dissolve the mixture and remove the TEA salts. Then, a vacuum filtration step is needed, to remove the TEA salts. The mixture needs to be, then, washed with hydrochloric acid, by the use of a

separation funnel. Sodium sulfate is added to the remaining organic mixture, for another cleaning step. Finally, ethyl acetate is removed, by a rotovapping step. The flask is placed on a rotary flask, in a water bath at 40 °C with a pressure of 99 mbar. Ethyl acetate is collected and the remaining mixture on the rotary flask is PGSA, to be collected. It can be stored in a refrigerator at 4°C, then properly injected into the mold and photocured by UV for 15 min on only one side.

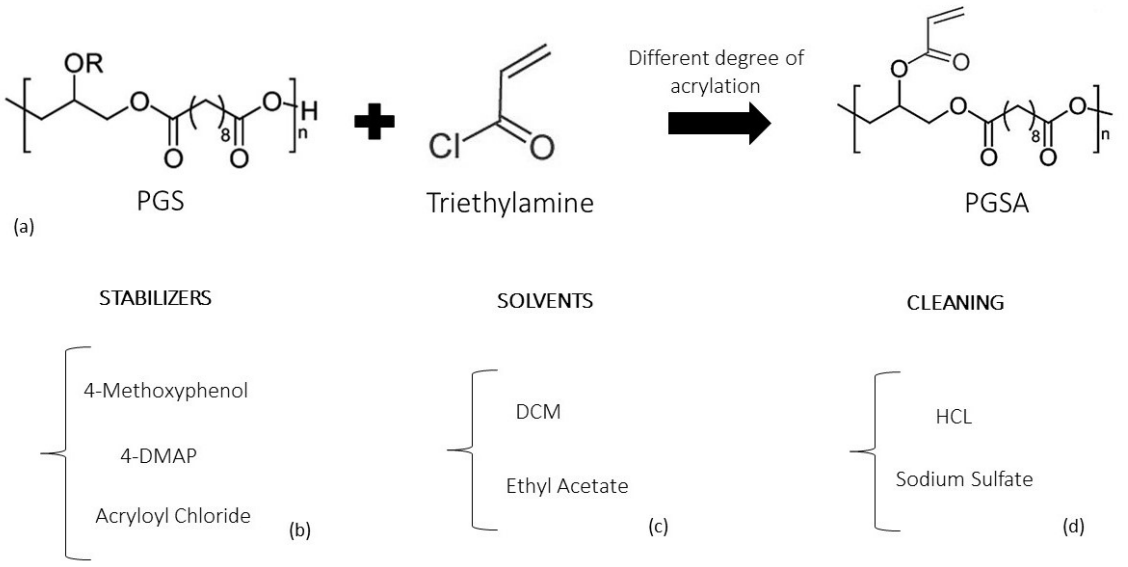

Figure 3.12: Acrylation process from PGS to PGSA; (a) Acrylation reaction; (b) Stabilizers chemicals; (c) Solvents; (d) Cleaning chemicals;

Fig3.12 show the crucial acrylation reaction and especially the main chemicals needed for the whole process.
In Fig3.13, some of the main synthesis steps are presented.

3.3.1.3 POMaC

The last chosen and synthesized material is POMaC - poly(octamethylene maleate (anhydride) citrate). This kind of polymer became quite common and start to diffuse fastly, thanks to the use of non-toxic monomers, a simple synthesis that can be conducted under mild conditions, that provide easy processability. Moreover, it is characterized by controllable mechanical properties and biodegradability, exhibiting non-toxic and minimal inflammatory properties *in vivo* [41].
This polymer is based on citric acid, maleic anhydride, and 1,8-octanediol, and the crosslinking can be both by photopolymerization and by polycondensation [42], [43].

The synthesis process is based on three main reactants: 1,8 octanediol, citric acid, and maleic anhydride; and it is characterized by two main steps: polycondensation and purification. They need to be mixed in a solution with molar ratio 5:1:4. They are added into a flask and placed on top of a heater. A N_2 flux is applied and the heater is turned on, at 140 °C. Moreover, a magnetic stir is added, to mix the reagents. The nitrogen flux need to be active for the duration of the process, which should last 3 h. Then, the heater should be turned off and the flask remove to cool down. A

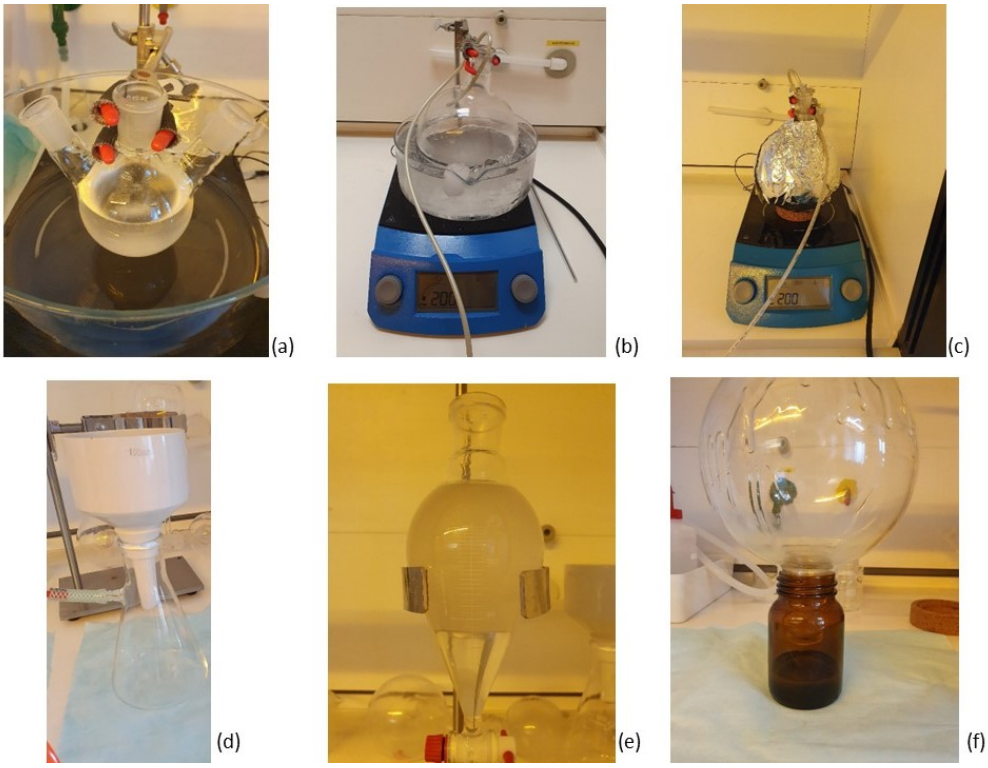

Figure 3.13: Main steps of PGSA synthesis; (a) Dissolve PGS with DCM; (b) Cool mixture down to 0°C with nitrogen flux; (c) Addition of TEA and AC, then leave the mixture for 24 hours at room temperature under the exclusion of light; (d) Vacuum filtration step to isolate the TEA salts; (e) HCl washing step; (f) Final collection of PGSA;

1,4 dioxane solvent needs to be added to dissolve the pre-POMaC, mixing it with a magnetic stir. Then the dissolved pre-polymer is poured into a separatory funnel, and placed on top of a baker with Milli-Q water. After the purification, pour the water out of the beaker, pre-POMaC stays at the bottom of it. Another important step is to apply overnight N2 flow is applied to the pre-POMaC inside the flask so that the residual water and 1,4-dioxane can be removed. Finally, the pre-POMaC is ready and can be stored, also for a long period of time in the refrigerator at 4°C, always protected from light.
Finally, mix POMaC prepolymer with PEGDM porogen at a 2:3 (POMaC/PEGDM porogen) weight ratio. Then, add 5% (wt/vol) initiator into the above mixture.
As the last step, the POMac can be injected into the PDMS mold and UV cured. For each side of the sample at least 20 min of curing are needed. However, also longer times are tried, to have more robust and less viscous samples.

3.3.2 Metal layer depostion

The metal layer deposition was for sure one of the most important steps. The adhesion on such kind of polymer was not assured and also check which kind of techniques best fit these materials was a target of the study.
Firstly, as expected, an adhesion layer, of PVA, was used, to improve the adhesion

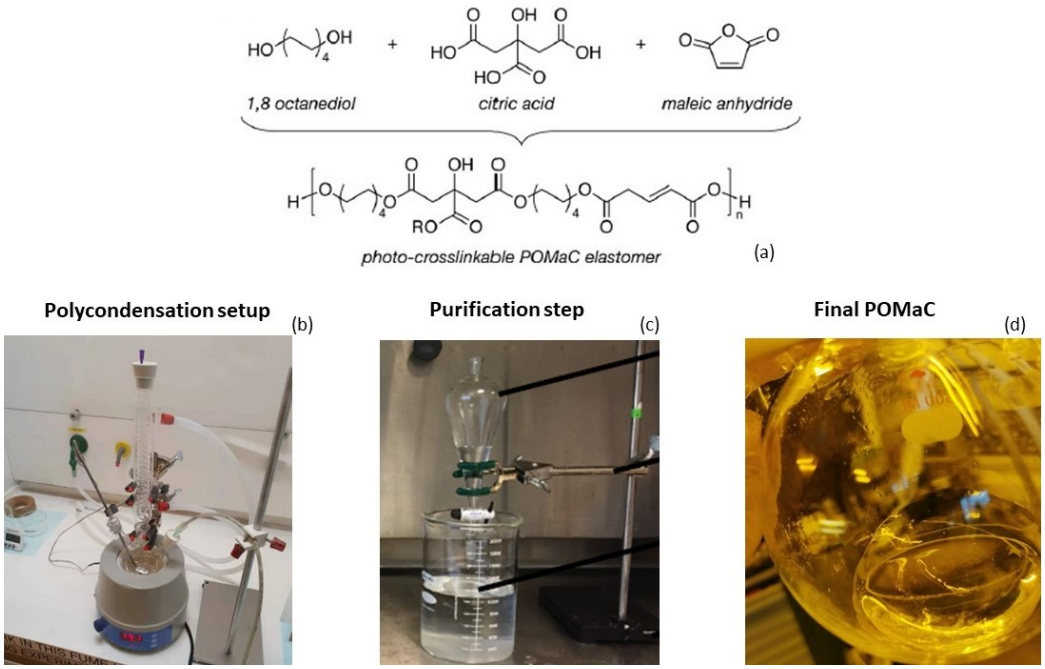

Figure 3.14: Main steps of POMaC synthesis and main reaction; (a) Chemistry of POMaC reaction [44]; (b) Polycondensation step; (c) Purification step; (d) Final transparent liquid POMaC;

and the quality of deposition on them. The evaporator was tried many times, but with larger and especially thicker samples it does not work, due to the degassing of these materials. For this reason, the spark ablation was the best and final solution to get the stretchable electrodes. Nonetheless, the evaporation was used on top of silicone-rubber layers just as a reference and test.

3.3.2.1 Iron PVD - Evaporation

One of the possible solutions was e-beam evaporation, a physical vapor deposition technique that allows the depositing of metal on top of the polymeric substrate. The utilized machine for this process was the CHA Smart Source Solution.
The working principle of the deposition process is quite straightforward: an electron beam produced in a bottom chamber of the machine and controlled by a series of magnets, hit the material to deposit, inside the crucible, heating it and causing an evaporation process, till the melting point. Once the target material reached its T_m it evaporates releasing ions that deposit on the substrate. Moreover, feedback on the deposition rate is possible thanks to a piezoelectric material, allowing, thus, to control the thickness of the deposited layer.

Iron was the chosen material due to its biocompatibility, however, one of the main drawbacks is its fast oxidation process.

To be able to have this kind of deposition, the CHA solution needs to reach

a high level of vacuum. The minimum one was about $2 * 10^{-6}$ mbar, to guarantee a good quality of the deposition. However, even if on some first tests on small size samples the deposition was feasible, using the real sample with 1 mm thicker and bigger *xy* dimensions, the machine can not reach the needed level of vacuum. This result was a bit expected, due to the possible degassing of the polymers.

On the other hand, both in the first test of deposition and in the test samples of soft silicone, the deposition rate was fixed at $1\frac{\text{Å}}{s}$, and with a very high level of vacuum, to have a better quality in the deposited layer.

3.3.2.2 Iron nanoparticle - Spark ablation

In the end, the deposition technique used to deposit a metal layer on top of the polymeric substrate is spark ablation, which allows having a uniform and dense layer of nanoparticles.
The working principle is based on the formation of sparks between two electrodes. These sparks have a small duration in time (a few microseconds) and generate a local and well-confined temperature of approximately 20000 K [45]. Due to this rapid increase, and to the extremely local nature of this high-temperature distribution, some hot spots are generated on the electrodes, where they are almost instantaneously heated up to the boiling point. Then, the vapor plume in the proximity of these electrodes is cooled, also thanks to a gas flow, that brings the particle to agglomerate.

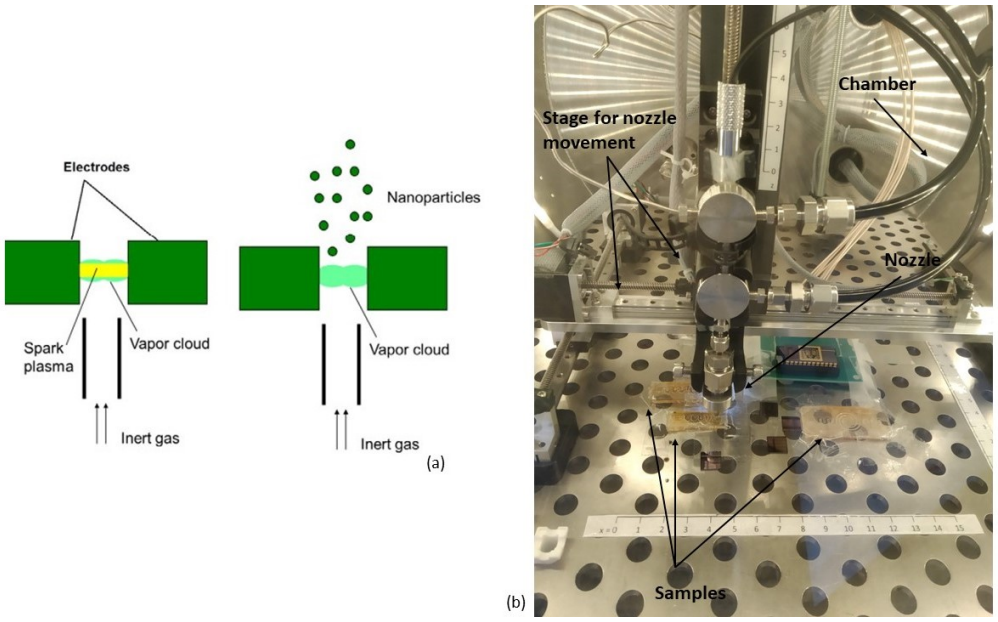

Figure 3.15: Theory of the spark ablation deposition and real chamber implementation; (a) Spark ablation between electrodes and vapor cloud [45]; (b) Real implemented chamber, with samples

Then to have the nanoparticle layer on the substrate, the sample needs to be fixed inside the plate of the chamber. Low pressure is applied (around 100 mtorr) just to improve the quality of the flux and deposition. Then the nozzle form in which the flux of nanoparticles comes out needs to be approximately aligned on top of the

sample. Firstly a vertical alignment is needed, to set the distance of deposition and also the focus for the camera. Finally, the alignment is executed on the xy plane. The shape of the deposition could be also programmed by controlling the movement of the nozzle. However in this case, due to the fact that the wanted shape is quite complex, and the controlling software allows only to print simple and basic shapes, the stencil masks need to be used anyway. The run code just prints a rectangle of the same xy dimension of the sample, with a printing speed of 40 mm/min, due to the high density of Fe nanoparticle that is generated by the spark. The voltage and current needed to generate the spark are respectively 1 kV and 3 mA. With this machine is, so, possible to have a pattern of Fe nanoparticles. Probably this kind of solution provides a lower conductivity than an e-beam evaporated layer, on the other hand, the nanoparticle nature of the layer should provide a better stretchability.

3.3.3 Process for fabrication

The overall fabrication process is quite straightforward, after the synthesis of the polymers. The main steps are the fabrication on the substrate, by PDMS mold, of the wanted dimension. In parallel, the stencil masks are prepared by the use of a precision blade cutter (Silhouette Cameo).
A PVA layer is then necessary to assure a better adhesion on the polymers. Finally, the metal deposition is made, by the use of the spark ablation machine. Thus, after that the pre-polymers are ready, some components need to be prepared, in particular: the polyamide masks, the PVA, and the PDMS molds.
The masks are simply cut from a foil of polyamide, in different wanted shapes. Moreover, before placing them on top of the samples, they are cleaned with IPA.
On the other hand, to get the PDMS mold firstly the PDMS (Sylgard 184) is prepared, by mixing the pre-polymer with the irrespective curing agent in a ratio 1:20. After mixing it is degassed for 30 min. In parallel mold with a 3D printer SLA are prepared and silanized.
The PDMS is then poured inside these molds and another step of degassing is needed, to improve the quality of the structure and its resistance.
Finally, the structure is cured for 2h at 80° C. The PDMS mold is then easily demolded.
Also, the PVA (Polyvinyl Alcohol) needs to be prepared. It is mixed in a 1% wt solution, mixed for 10 min, and then mixed for another 30 min at 80°C, to have a better solubility. Finally, once every part is ready and assuming that the polymers (POMaC, PGS, and PGSA) are ready they are firstly degassed and then:

1. the polymers are poured inside the PDMS mold (previously silanized) through a syringe;
2. after the pouring step another degassing process for 30 min is executed;
3. the PDMS mold + poured polymer are cured by the proper method and time;
4. the polymeric substrate is then easily demolded
5. the masks are placed on top of the substrate; the polymeric parallelepiped is quite sticky (especially in the case of POMaC and PGSA), guaranteeing a good

adhesion between the mask and the substrate

6. PVA is then distributed on top of the device through a pipette;
7. the deposition is made by the spark ablation method
8. finally the mask is pulled off and the stretchable electrodes with the metal nanoparticles metal on top are ready;

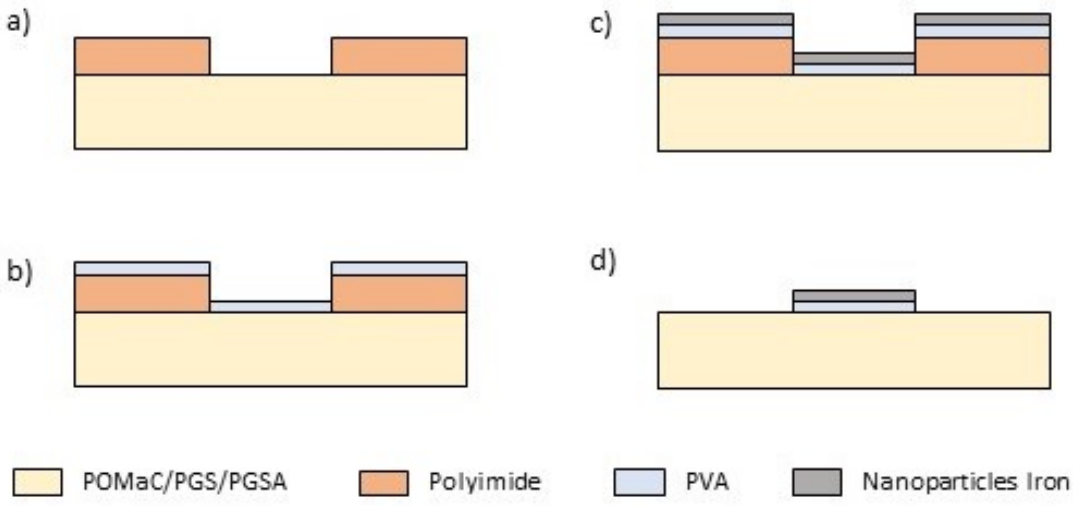

Figure 3.16: Process flow of the fabrication of the stretchable electrodes; (a) Polymeric substrate and stencil mask; (b) PVA distribution; (c) Spark ablation of Fe nanoparticle; (d) Stencil mask pilled off, final device

Part of the project was, then, also to try and work on the microfabrication techniques of these polymers. The deposition by e-beam evaporation was tested in the first moment on a small sample, also to check the adhesion and the quality of deposition. However, with thicker and larger samples, problems with degassing are present. On the other hand, especially with POMaC the cleaning step with oxygen plasma has been noticed to affect a bit the quality of the surface.
For all these reasons, and to have a more reliable and feasible process, the spark ablation was chosen. Nevertheless, the main drawbacks techniques are:
- only a limited number of samples can be executed in the same process, and it is much more time-consuming, also for the programming part, due to the fact that for each sample a planar alignment is needed;
- the contact on a nanoparticles layer could be much more difficult and less stable. The best solution could be to have a metal pad, made by evaporation and a nanoparticle pattern, with the use of two masks. However, this approach could not be tested

due to the degassing problem with CHA Solution.

Finally, also the handling with this type of polymers (especially POMaC and PGSA) is quite hard. They are extremely sticky and also not easy to move. For these reasons also different curing times and thicknesses are tested, trying to reach the best properties for the specific application, so as to have a handle substrate, sufficiently robust, and elastic.

3.4 Characterization

After the fabrication of the samples, two types of characterization were executed. General analysis on the surface, with SEM and laser scanner microscope. Especially this acquisition was performed on the samples with spark ablation, to check the density, quality, and characteristics of the nanoparticle layer.
Another type of characterization was to really test the behavior of the electrodes, so, how the capacitance change as a function of the strain. To do that a setup was built. This setup was composed of a linear stage and fully controlled by an Arduino and Labview code, that, through the control of the motor and of an LCR meter, permitted the stretch of the sample and contemporary the acquisition of the capacitance, as a function of the strain. For better accuracy, the basic capacitance was acquired with a probe station. Then the capacitance vs strain curve was extracted with this hand-made setup.
Nevertheless, even if the setup was working, the small expected variation in capacitance and the noisy system (due to parasitic capacitance and not completely isolated and stable stage) affect in a relevant way the measure. These results are not completely reliable, due to the high ratio of noise and low stability of the characterization.

3.4.1 Surface analysis

After the deposition, to check the quality of the layer and to better visualize the metal structure, images with SEM and a Keyence microscope are taken.

In particular Fig. 3.17 it is focused on a crack between iron grains. This crack affects the conductivity of the pattern and especially decreases the performance when a strain is applied, increasing the resistance, especially when several cycles are involved.

On the other hand, it was quite interesting to visualize the nanoparticle layer on the polymeric substrate. Fig.3.18 and Fig.3.19 show a dense layer of Fe nanoparticle. This images acquisition was especially to check that the layer of nanoparticle was sufficiently dense.

3.4.2 Impedence and stretchability

To test and extract how the capacitance change with the stretch on the sample, a setup needed to be built. The aim of the setup was quite simple, stretch the sample and acquire the capacitance for a different applied strain.

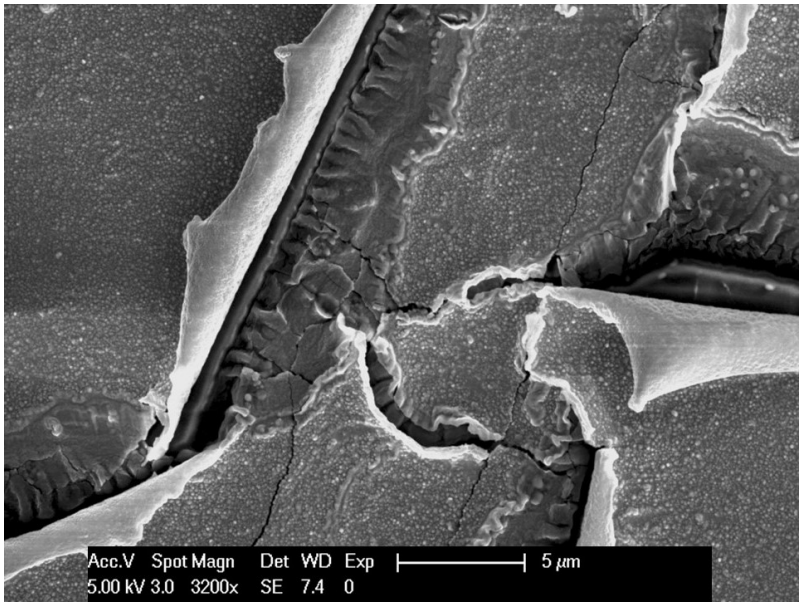

Figure 3.17: SEM images on a Fe crack deposited by e-beam evaporation, on a POMaC test sample

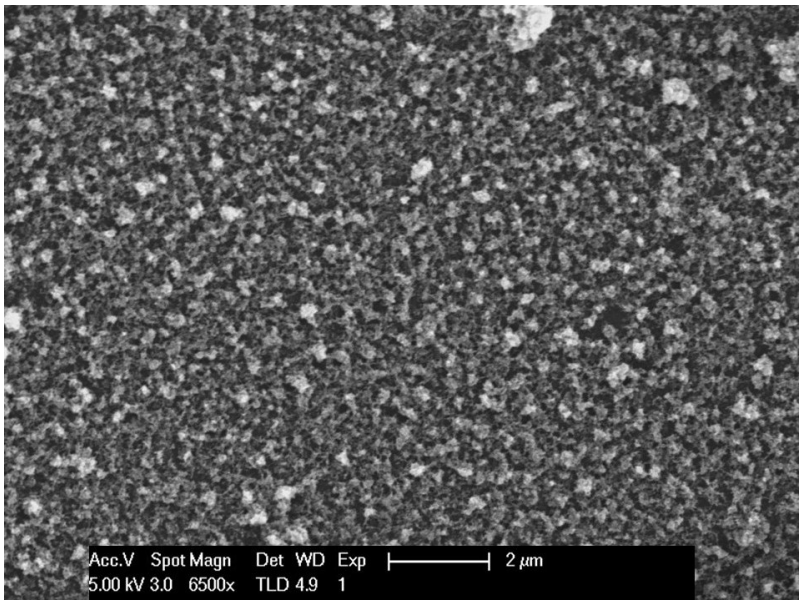

Figure 3.18: SEM images of Fe nanoparticle on PGS (higher scale);

The overall system is based on a linear stage, on which the sample is placed and stretched, and an LCR meter for the capacitance measure.
The system is controlled by an Arduino and Labview code.

3.4.2.1 Setup

To develop such kind of setup, firstly, a definition of the needed components is crucial. The main parts can be summarized: a linear stage with a stepper motor to stretch and elongate the sample, a motor driver to correctly interface from an

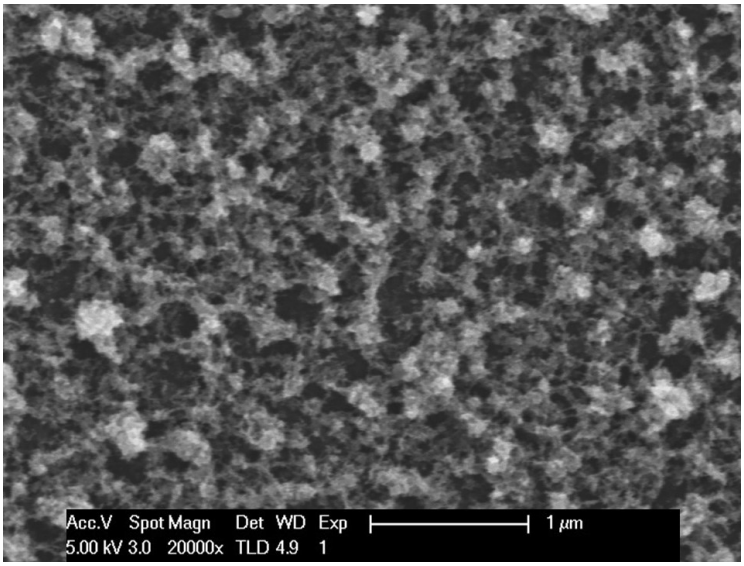

Figure 3.19: SEM images of Fe nanoparticle on PGS (lower scale);

electrical point of view with the stepper motor, and a microcontroller to control the motor and send the proper signal, an LCR meter for the capacitance (and in general impedance) acquisition, a power supply for motor driver. Then, after an analysis of the specification of the systems and of the single components, the selected parts are:

- linear stage Newport with a stepper motor NEMA 17 and length pitch of 2 mm (a complete rotation of the motor moves the stage of 2 mm), with optionally a rotary encoder;
- TB6600 as motor driver, that can properly interface both with the NEMA 17 stepper motor and Arduino
- Arduino Due board as microcontroller
- Agilent 4284A Precison LCR meter
- Aim-TTi CPX400DP Power Supply

Then the systems need to be set up and properly connected. The motor driver needs to be connected between the Arduino board and the stepper motor. The connection between the Arduino and the motor driver is in a common anode configuration. As input, the motor driver has 6 signals (ENA+, ENA-, DIR+, DIR-, PUL+, PUL-). In the common anode, all the minus signals are connected to the ground, while the other three (positive) are connected to Arduino. The three pins of the microcontroller are set as input. The ENA+ is kept always LOW, while the two other signals control the direction of the rotation and the rotation itself (if moves or not). Finally, the motor driver is connected to the stepper motor and alimented with the proper value of voltage. Moreover, the switches of the motor driver need to be set depending on the characteristics of the motor (number of steps and current).

Moreover, on the Newmark linear stage, an optical rotary encoder was included. This component was used with the aim to detect the limit of the stage, so when the

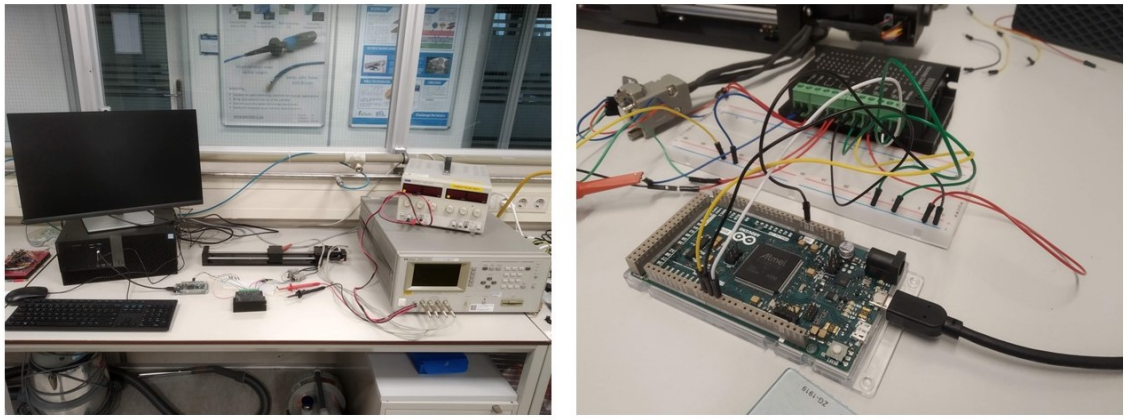

(a) (b)

Figure 3.20: Setup for impedance extraction with the application of strain; (a) General setup; (b) Connection between Arduino Due board and TB6600 motor driver

plate had reached the extreme limit of the pitch and can not move over. The optical rotary encoder needs to be alimented (+5 V) and it gives as output two signals, that go as input to the Arduino board. Analyzing these signals it is possible to detect the eventual movement of the motor and the direction.

Then the development of an Arduino and Labview code was for sure a crucial part. The code allows setting the length of the sample, the maximum strain, and the number of cycles, eventually, stretching the samples. Then the LCR meter is also controlled by the Labview system and the wanted parameters are acquired.
In the case under study, to limit the considerable noise, the samples were stretched to well define strain, and several data are acquired, to have larger statistics and, computing the standard deviation, reduce the noise.
Thus, what was done to extract how the capacitance changed as a function of the strain: the samples were fixed on the linear stage and stretched to some specified strains, then the LCR meter acquired many capacitance measures, and analyzed in post-processing to extract the mean and the standard deviation. In such a way was possible to estimate the variation of the capacitance as a function of the elongation.

3.4.2.2 Capacitance and stretching results

Finally, the characterization of the capacitance was performed. The targets of this phase were to extract the basic capacitance, compare it with the theoretical one, and see the behavior of the capacitance itself depending on the strain of the samples.
However, this phase was executed especially to conclude and have a first idea about the designed and fabricated stretchable electrode. Due to the different tests and difficulties during the fabrication, a very low number of samples could be really characterized. In particular, the goal was to have one sample for a type of substrate and structure, to have a first idea of the different behavior, concerning both the different materials and structures (interdigitated and spirals). This aspect makes the data less reliable but provides a conclusion and a first characterization of the developed sensors.

SPIRALS	Capacitance (pF)
Simulation	0.816
PGS	0.724
PGSA	0.786
POMaC	0.803
Silicone-rubber	1.057

(a)

INTERDIGITATED	Capacitance (pF)
Simulation	0.245
PGS	0.228
POMaC	0.258
Silicone-rubber	0.301

(b)

Figure 3.21: Summary of basic capacitance for spirals and interdigitated samples on different substrates; (a) Concentric spirals structure; (b) Interdigitated structure

In particular, Fig3.21 show the different basic capacitance C_0 for each substrate and type of sensor. The measure was executed through a probe station, to have better accuracy.
What emerges is that the experimental capacitance is quite close to the theoretical one. The silicone-rubber layer, fabricated as a test, shows the bigger difference. Probably due to not good adhesion of the mask on the substrate (not sticky), that has changed and affected the final shape and dimensions. On the other hand, the other capacitance is quite close to the one computed by Comsol. This is quite relevant, taking into account that in this case the metal layer is made by a dense agglomerate of nanoparticles.

Then, the samples are characterized on the hand-made setup. One of the main problems in this phase was the fact the expected variation of the capacitance was in the order of tens of fF, so the setup need to guarantee high precision and stability.

Fig 3.22 show the main behaviour for the different substrates. It is important to note how the maximum strain applicable is different for each material because each of them starts to break at different points. In particular POMaC, for the way in which was synthesized, was shown to be more brittle and less elastic.
What emerges from this analysis is that in general is possible to see the expected trend, so a first decreasing phase and an increasing one later. However, as expected, the variation of the capacitance (and the basic capacitance itself) are too small to be accurately measured by the setup. The standard deviation of the measure is around a few fF, making this data not very reliable.
The same was for the interdigitated structures, in which the monotonic decreasing trend can be extracted, but it is difficult to have a more detailed analysis.

Nevertheless, these results are a good starting point for future work. The structure could be improved, and the basic capacitance is quite close to the expected. For sure some improvements to the setup and especially the stage are needed, especially to make it more stable and less noisy.

3.5 Discussion

Finally, different stages in the development of biodegradable stretchable electrodes were developed.

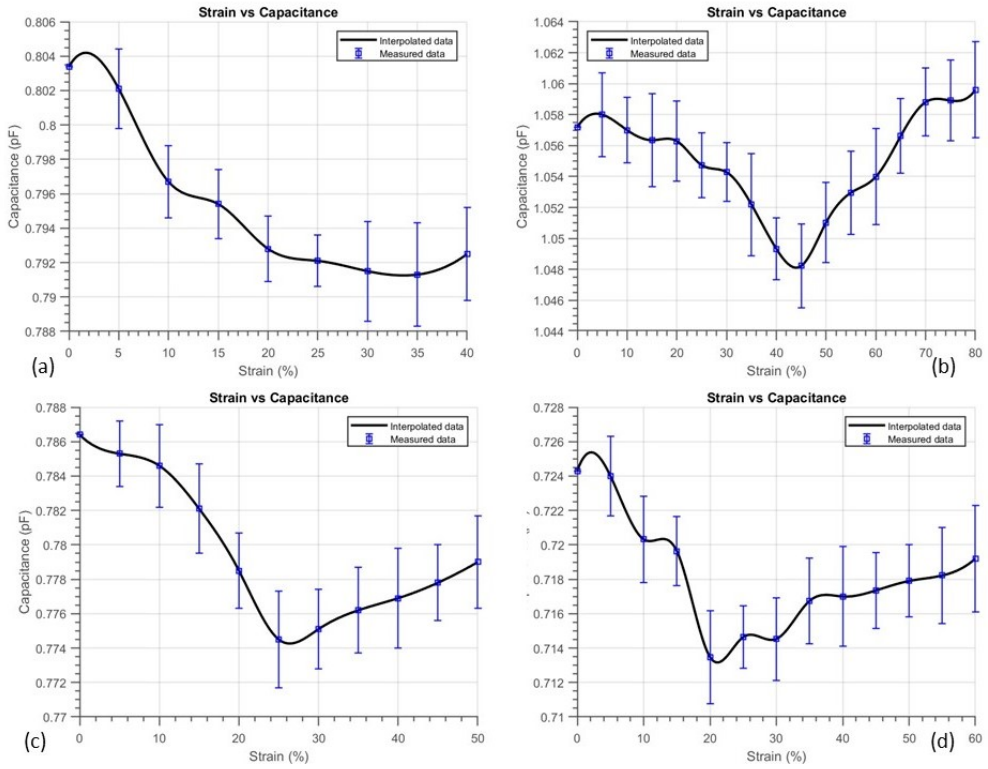

Figure 3.22: Variation of the capacitance as a function of the applied strain for a different material for spiral structure; (a) Capacitance variation on POMaC substrate with strain; (b) Capacitance variation on soft silicone substrate with strain; (c) Capacitance variation on PGSA substrate with strain; (d) Capacitance variation on PGS substrate with strain;

Three biodegradable materials are synthesized (POMaC, PGS, and PGSA), better defining their protocols and making them suitable for this kind of application.
The second phase of design was performed, and, especially, two capacitive strain sensing patterns were developed: interdigitated and concentric spirals. These two different solutions could be suitable to be used as strain sensors, but the performances (such as basic capacitance and sensitivity) could be improved with a change in the geometrical dimensions, that in this case were also limited by the resolution of the stencil mask.
Moreover, microfabrication techniques are tested with these materials, being aware of the possible issues. For these reasons, spark ablation seemed to be the most suitable deposition technique.
Finally, some devices are fabricated, especially to test the hand-made setup for the capacitance-strain curve extraction, and to check the behavior and the limit of the systems. The final data are not completely reliable due to a low number of samples and statistics and the high noise (standard deviation) associated with the measure, with respect to the capacitance variation.

Overall, all the initial targets of the project were reached, also it was a great result to have characterizable devices.

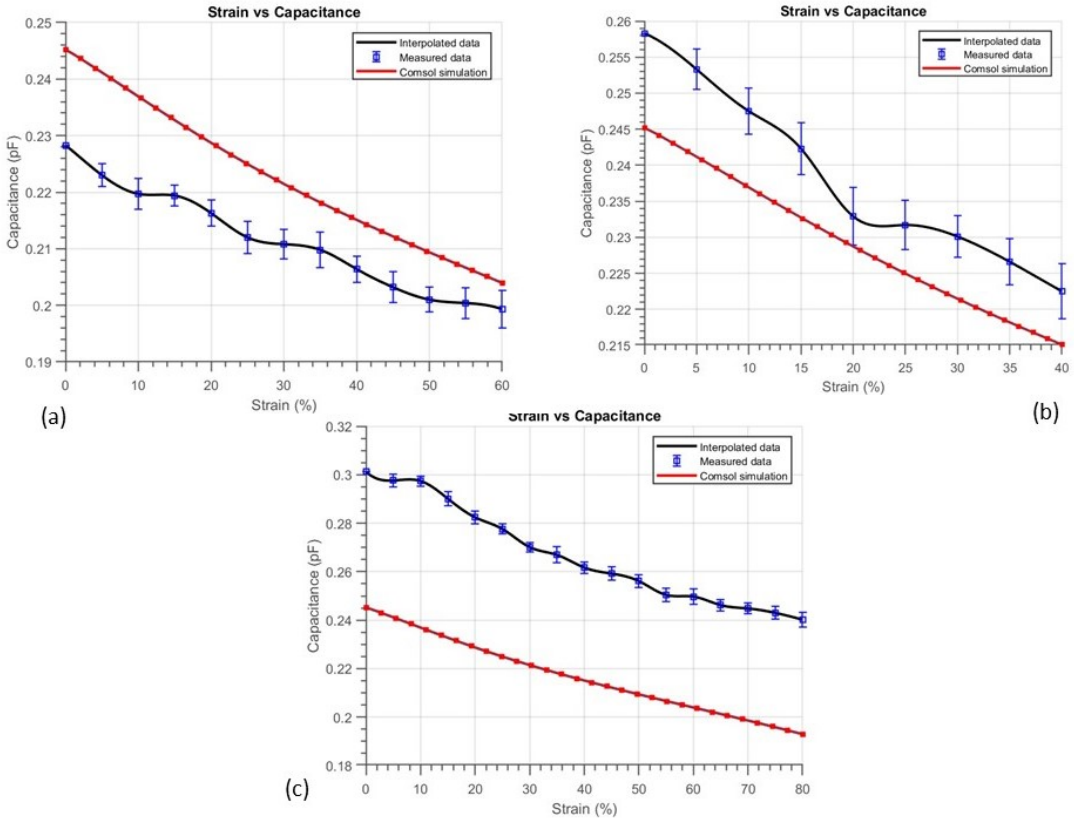

Figure 3.23: Variation of the capacitance as a function of the applied strain for a different material for interdigitated structure; (a) Capacitance variation on PGS substrate with strain ; (b) Capacitance variation on POMaC substrate with strain; (c) Capacitance variation on silicone substrate with strain;

Firstly the definition of the synthesis process for the three polymers and having a handle and suitable substrate for this kind of application was the first accomplishment. Moreover, testing the limit and issues of microfabrication techniques on them, such as the problem of degassing or etching during the oxygen plasma cleaning, provide useful information for future work.
The definition and design of capacitive strain patterns, stretchable and suitable for planar strain sensors was another important point, even if, in this case, some aspects could be improved, especially on the final dimension. The use of a photolithography process could increase the resolution and quality of the pattern, increasing then the sensitivity of the sensor itself. However, already have reached the definition of two different working structures were great results.
Last but not least the construction of the setup and its testing was a final important step, especially to highlight its limit and future improvement. The final extracted result, as expected are not reliable, but provides a relevant starting point to continue the work and better develop the fixed milestones. Overall, it was good to define a suitable microfabrication process flow with these materials and also tho check the correspondence between the expected and measured capacitance. Nevertheless, the capacitance vs strain curves is not reliable due to the large variation in the

measurement compered to the expected one.

Chapter 4

Conclusion

This master's thesis project is inserted in a bigger context, the development of a biodegradable scaffold for peripheral nerve regrow. However, the big project in which it is inserted starts from scratch and the main components and parts need to be set. For this reason, the project itself is divided into two sub-section, that run in parallel. Both of them have the aim to set the basics for the continuation of the scaffold work.

Platform for Organ-on-Chip mechanobiological analysis In this first part, all the steps are executed. A platform was designed and optimized, also taking into account the most suitable hyperelastic models to use. After optimization in the fabrication and assembly process, the real characterization was performed, by the use of the Digital Image Correlation technique, a hand-made setup, and Matlab code. The extensive characterization and testing of the device were especially to check its behavior and the failure rate. Finally, a biological study was executed, to check the biocompatibility and the real strain sensed by the cells.
Overall, good results are got. The final device behaves following the expected behavior. However, some improvements need to be performed especially to improve the quality of the data and their accuracy. The experimental strain, even if is quite close to the theoretical one, needs to be better analyzed, increasing and optimizing the image acquisition and analysis process, also maybe executing a more extensive biological study.

Biodegradable stretchable electrodes In this second part of the project, the real basic components of a stretchable biodegradable electrode are the aspects under investigation. Several aspects are studied and tested. Firstly three different suitable biodegradable materials are synthesized, to have a larger availability of possible stretchable substrates. Then the conductive pattern, able to sense the strain by a capacitive variation was designed. However, in this case, the overall dimensions are limited by the resolution on the stencil mask, so a photolithographic process could increase the overall performance. However, the design of these stretchable patterns was for sure another relevant accomplishment.
A fabrication step was then tried and optimized, and as the final choice, a Fe layer by spark ablation was chosen as the conductive line. Also in this case several attempts

were made to test and check the best microfabrication technique with these polymers and observe the main issues and limits. Finally, a setup to stretch the samples and measure the impedance was built. This setup was tested on a limited number of samples. However, this phase of the characterization shows the main limitations of the setup (noise) but also confirms the expected trend in the capacitance variation. Nevertheless, in this case, it is not possible to add many conclusions due to the low reliability of the extracted data.
Thus, several basic steps are prepared and analyzed for the future development of such devices: the synthesis process of three different polymers, the general behavior of two different capacitive strain sensors, a better understanding of the limitation and issues of microfabrication techniques with these material and a setup to characterized them (to be improved in term of accuracy).

Acknowledgements

It is a great pleasure to thank everybody who made this thesis possible. I owe my gratitude to my advisor, Prof. Clementine Boutry for her invaluable guidance and constant support throughout the course of my research duration. I am also immensely grateful to the TU Delft and EKL Lab to give me the opportunity to collaborate with them and for their hospitality.

I am very pleased to thank the Polytechnic of Turin to give me the opportunity of undertaking Master Studies at this highly esteemed institution and extend the financial support for this project.

I am extremely grateful to my girlfriend Aurora, for the continuous support and encouragement, and for the great patience. She has motivated me in the last two years and helped me to overcome all the tough moments despite the distance, I will be forever grateful.
Last but not least a special thanks to Francesco and Mattia, for all the support and the beautiful moments spent together, making everything easier and unforgettable.

A real special thanks to Dr. Del Medico and Dr. Balatsinou. When I started I was well aware of the difficulties that two chronic autoimmune diseases would have brought me, it would not have been easy to embark on and conclude such kind of path, but thanks to their support and constant supervision even something that seemed impossible ended successfully.

Bibliography

[1] Valentina Paggi, Outman Akouissi, Silvestro Micera, and Stéphanie P Lacour. «Compliant peripheral nerve interfaces». In: *Journal of Neural Engineering* 18.3 (2021), p. 031001 (cit. on p. 1).

[2] AP Balgude, X Yu, A Szymanski, and RV Bellamkonda. «Agarose gel stiffness determines rate of DRG neurite extension in 3D cultures». In: *Biomaterials* 22.10 (2001), pp. 1077–1084 (cit. on p. 1).

[3] Alessandro Faroni, S Atefeh Mobasseri, Paul J Kingham, and Adam J Reid. «Peripheral nerve regeneration: experimental strategies and future perspectives». In: *Advanced drug delivery reviews* 82 (2015), pp. 160–167 (cit. on p. 1).

[4] Jong-Hoon Park, Takashi Ushida, and Takayuki Akimoto. «Control of cell differentiation by mechanical stress». In: *The journal of physical fitness and sports medicine* 2.1 (2013), pp. 49–62 (cit. on p. 4).

[5] Mustafa Unal et al. «Micro and nano-scale technologies for cell mechanics». In: *Nanobiomedicine* 1.Godište 2014 (2014), pp. 1–5 (cit. on p. 4).

[6] Deok-Ho Kim, Pak Kin Wong, Jungyul Park, Andre Levchenko, and Yu Sun. «Microengineered platforms for cell mechanobiology». In: *Annual review of biomedical engineering* 11.1 (2009), pp. 203–233 (cit. on p. 4).

[7] Thomas D Brown. «Techniques for mechanical stimulation of cells in vitro: a review». In: *Journal of biomechanics* 33.1 (2000), pp. 3–14 (cit. on p. 4).

[8] Yun Jung Heo, Tetsuo Kan, Eiji Iwase, Kiyoshi Matsumoto, and Isao Shimoyama. «Stretchable cell culture platforms using micropneumatic actuators». In: *Micro & Nano Letters* 8.12 (2013), pp. 865–868 (cit. on pp. 5, 29).

[9] Chaitanya Prashant Ursekar, Soo-Kng Teo, Hiroaki Hirata, Ichiro Harada, Keng-Hwee Chiam, and Yasuhiro Sawada. «Design and construction of an equibiaxial cell stretching system that is improved for biochemical analysis». In: *PloS one* 9.3 (2014), e90665 (cit. on p. 5).

[10] A Colombo, PA Cahill, and C Lally. «An analysis of the strain field in biaxial Flexcell membranes for different waveforms and frequencies». In: *Proceedings of the Institution of Mechanical Engineers, Part H: Journal of Engineering in Medicine* 222.8 (2008), pp. 1235–1245 (cit. on p. 5).

[11] John Case and Amos Henry Chilver. *Strength of materials: an introduction to the analysis of stress and strain*. Elsevier, 2013 (cit. on p. 7).

[12] Tomasz Wierzbicki. *Structural Mechanics*. MIT -libreTexts, 2021 (cit. on p. 7).

[13] Michael Fagan and Michiel Postema. *Introduction to stress and strain analysis*. The University of Hull, 2007 (cit. on p. 8).

[14] Hossein B Khaniki, Mergen H Ghayesh, Rey Chin, and Marco Amabili. «A review on the nonlinear dynamics of hyperelastic structures». In: *Nonlinear Dynamics* (2022), pp. 1–32 (cit. on p. 8).

[15] Stephen K Melly, Liwu Liu, Yanju Liu, and Jinsong Leng. «A review on material models for isotropic hyperelasticity». In: *International Journal of Mechanical System Dynamics* 1.1 (2021), pp. 71–88 (cit. on pp. 9, 10).

[16] Jorgen S Bergstrom. *Mechanics of solid polymers: theory and computational modeling*. William Andrew, 2015 (cit. on p. 9).

[17] Melvin Mooney. «A theory of large elastic deformation». In: *Journal of applied physics* 11.9 (1940), pp. 582–592 (cit. on p. 9).

[18] Ronald S Rivlin. «Large elastic deformations of isotropic materials IV. Further developments of the general theory». In: *Philosophical transactions of the royal society of London. Series A, Mathematical and physical sciences* 241.835 (1948), pp. 379–397 (cit. on p. 9).

[19] Raymond William Ogden. «Large deformation isotropic elasticity–on the correlation of theory and experiment for incompressible rubberlike solids». In: *Proceedings of the Royal Society of London. A. Mathematical and Physical Sciences* 326.1567 (1972), pp. 565–584 (cit. on p. 10).

[20] LRG Treloar. «Stress-strain data for vulcanized rubber under various types of deformation». In: *Rubber Chemistry and Technology* 17.4 (1944), pp. 813–825 (cit. on p. 10).

[21] WH Peters and WF Ranson. «Digital imaging techniques in experimental stress analysis». In: *Optical engineering* 21.3 (1982), pp. 427–431 (cit. on p. 21).

[22] Nick McCormick and Jerry Lord. «Digital image correlation». In: *Materials today* 13.12 (2010), pp. 52–54 (cit. on p. 21).

[23] Per-Erik Austrell, Bertil Enquist, Anders Heyden, and Sven Spanne. «Contact free strain measurement using MATLAB image processing toolbox». In: *Nordic MATLAB Conference, Stockholm*. Citeseer. 1995 (cit. on p. 21).

[24] J Blaber, B Adair, and A Antoniou. «Ncorr: open-source 2D digital image correlation matlab software». In: *Experimental Mechanics* 55.6 (2015), pp. 1105–1122 (cit. on pp. 21, 22).

[25] Xin Meng, Lex Huismans, Teun Huijben, Greta Szabo, Ruud Van Tol, Izak De Heer, Srividya Ganapathy, and Daan Brinks. «A compact microscope for voltage imaging». In: *Journal of Optics* 24.5 (2022), p. 054004 (cit. on p. 28).

[26] Sara Pérez Davila, Laura González Rodrıguez, Stefano Chiussi, Julia Serra, and Pıo González. «How to sterilize polylactic acid based medical devices?» In: *Polymers* 13.13 (2021), p. 2115 (cit. on p. 29).

[27] Fahima Akther, Shazwani Binte Yakob, Nam-Trung Nguyen, and Hang T Ta. «Surface modification techniques for endothelial cell seeding in PDMS microfluidic devices». In: *Biosensors* 10.11 (2020), p. 182 (cit. on p. 29).

[28] Ji-Hun Seo, Keiko Sakai, and Nobuhiko Yui. «Adsorption state of fibronectin on poly (dimethylsiloxane) surfaces with varied stiffness can dominate adhesion density of fibroblasts». In: *Acta biomaterialia* 9.3 (2013), pp. 5493–5501 (cit. on p. 29).

[29] Siya Huang, Yuan Liu, Yue Zhao, Zhifeng Ren, and Chuan Fei Guo. «Flexible electronics: stretchable electrodes and their future». In: *Advanced Functional Materials* 29.6 (2019), p. 1805924 (cit. on p. 34).

[30] Hong Hocheng and Chao-Ming Chen. «Design, fabrication and failure analysis of stretchable electrical routings». In: *Sensors* 14.7 (2014), pp. 11855–11877 (cit. on pp. 35, 37).

[31] Yujeong Lee, Minkwan Shin, Kaliannan Thiyagarajan, and Unyong Jeong. «Approaches to stretchable polymer active channels for deformable transistors». In: *Macromolecules* 49.2 (2016), pp. 433–444 (cit. on pp. 35, 37).

[32] Yumeng Wang, Xingsheng Li, Yue Hou, Chengri Yin, and Zhenxing Yin. «A review on structures, materials and applications of stretchable electrodes». In: *Frontiers of Materials Science* 15.1 (2021), pp. 54–78 (cit. on p. 35).

[33] Morteza Amjadi, Ki-Uk Kyung, Inkyu Park, and Metin Sitti. «Stretchable, skin-mountable, and wearable strain sensors and their potential applications: a review». In: *Advanced Functional Materials* 26.11 (2016), pp. 1678–1698 (cit. on p. 35).

[34] Seung-Rok Kim, Jin-Hoon Kim, and Jin-Woo Park. «Wearable and transparent capacitive strain sensor with high sensitivity based on patterned Ag nanowire networks». In: *ACS applied materials & interfaces* 9.31 (2017), pp. 26407–26416 (cit. on pp. 35, 36).

[35] A Fassler and C Majidi. «Soft-matter capacitors and inductors for hyperelastic strain sensing and stretchable electronics». In: *Smart Materials and Structures* 22.5 (2013), p. 055023 (cit. on pp. 35, 36).

[36] Lena Vogt, Florian Ruther, Sahar Salehi, and Aldo R Boccaccini. «Poly (glycerol sebacate) in biomedical applications—A review of the recent literature». In: *Advanced Healthcare Materials* 10.9 (2021), p. 2002026 (cit. on p. 44).

[37] Ranjana Rai, Marwa Tallawi, Alexandra Grigore, and Aldo R Boccaccini. «Synthesis, properties and biomedical applications of poly (glycerol sebacate)(PGS): A review». In: *Progress in polymer science* 37.8 (2012), pp. 1051–1078 (cit. on p. 45).

[38] Yadong Wang, Guillermo A Ameer, Barbara J Sheppard, and Robert Langer. «A tough biodegradable elastomer». In: *Nature biotechnology* 20.6 (2002), pp. 602–606 (cit. on p. 44).

[39] Jamie L Ifkovits, Robert F Padera, and Jason A Burdick. «Biodegradable and radically polymerized elastomers with enhanced processing capabilities». In: *Biomedical materials* 3.3 (2008), p. 034104 (cit. on p. 45).

[40] Christiaan LE Nijst, Joost P Bruggeman, Jeffrey M Karp, Lino Ferreira, Andreas Zumbuehl, Christopher J Bettinger, and Robert Langer. «Synthesis and characterization of photocurable elastomers from poly (glycerol-co-sebacate)». In: *Biomacromolecules* 8.10 (2007), pp. 3067–3073 (cit. on p. 45).

[41] Miles Montgomery et al. «Flexible shape-memory scaffold for minimally invasive delivery of functional tissues». In: *Nature materials* 16.10 (2017), pp. 1038–1046 (cit. on p. 46).

[42] Richard T Tran, Paul Thevenot, Dipendra Gyawali, Jung-Chih Chiao, Liping Tang, and Jian Yang. «Synthesis and characterization of a biodegradable elastomer featuring a dual crosslinking mechanism». In: *Soft matter* 6.11 (2010), pp. 2449–2461 (cit. on p. 46).

[43] Boyang Zhang, Benjamin Fook Lun Lai, Ruoxiao Xie, Locke Davenport Huyer, Miles Montgomery, and Milica Radisic. «Microfabrication of AngioChip, a biodegradable polymer scaffold with microfluidic vasculature». In: *Nature protocols* 13.8 (2018), pp. 1793–1813 (cit. on p. 46).

[44] Vivian R Feig, Helen Tran, and Zhenan Bao. «Biodegradable polymeric materials in degradable electronic devices». In: *ACS central science* 4.3 (2018), pp. 337–348 (cit. on p. 48).

[45] TV Pfeiffer, J Feng, and A Schmidt-Ott. «New developments in spark production of nanoparticles». In: *Advanced Powder Technology* 25.1 (2014), pp. 56–70 (cit. on p. 49).